NATIONAL POLAR-ORBITING OPERATIONAL ENVIRONMENTAL SATELLITE SYSTEM (NPOESS)

VIIRS SNOW COVER ALGORITHM THEORETICAL BASIS DOCUMENT (ATBD) (D43758 Rev B)

CDRL No. A032

Northrop Grumman Space & Mission Systems Corporation
One Space Park
Redondo Beach, California 90278

Copyright © 2004-2010
Northrop Grumman Corporation and Raytheon Company
Unpublished Work
ALL RIGHTS RESERVED

Portions of this work are the copyrighted work of Northrop Grumman and Raytheon. However, other entities may own copyrights in this work.

This documentation/technical data was developed pursuant to Contract Number F04701-02-C-0502 with the US Government. The US Government's rights in and to this copyrighted data are as specified in DFAR 252.227-7013, which was made part of the above contract.

This document has been identified per the NPOESS Common Data Format Control Book – External Volume 5 Metadata, D34862-05, Appendix B as a document to be provided to the NOAA Comprehensive Large Array-data Stewardship System (CLASS) via the delivery of NPOESS Document Release Packages to CLASS.

The information provided herein does not contain technical data as defined in the International Traffic in Arms Regulations (ITAR) 22 CFR 120.10.

This document has been approved by the Unites States Government for public release in accordance with NOAA NPOESS Integrated Program Office.

Distribution: Statement A: Approved for public release; distribution is unlimited.

D43758, B. PDMO Released: 2010-06-22 (VERIFY REVISION STATUS)
PDMO

NATIONAL POLAR-ORBITING OPERATIONAL ENVIRONMENTAL SATELLITE SYSTEM (NPOESS)

VIIRS SNOW COVER ALGORITHM THEORETICAL BASIS DOCUMENT (ATBD) (D43758 Rev B)

ELECTRONIC APPROVAL SIGNATURES:

_____

Roy Tsugawa Date
Algorithm & Data Processing IPT Lead &
Algorithm Change Control Board Chairperson

_____

Ben James Date
Operations & Support IPT Lead

The following individuals are recognized for their contributions to the current or previous versions of this document.

Robert Mahoney

Ken Jensen

Igor Appel

D43758, B. PDMO Released: 2010-06-22 (VERIFY REVISION STATUS)
PDMO

Revision/Change Record

Document Number D43758

Revision	Document Date	Revision/Change Description	Pages Affected
---	1/24/2007	Initial PCIM Release to bring document into Matrix Accountability. Reference original document number: Y2401 delivered in 2005	All

D43758, B. PDMO Released: 2010-06-22 (VERIFY REVISION STATUS)
PDMO

Revision/Change Record

Document Number D43758

Revision	Document Date	Revision/Change Description	Pages Affected
A	03/06/2007	Rev-A revisions associated with snow cover algorithm modifications to allow processing over fresh water lakes (inland water and coastal pixels) made under SPCRs 1116 and 1131. Added clarifications to state that the Multiple End Member Spectral Analysis (MESMA) algorithm for computing snow fraction has been developed but is not being implemented operationally. Also made minor document corrections where appropriate. 1. Replaced "Surface Type" in the title with "Snow Cover" on page ii 2. Added "Revision A" to first sentence of Abstract on page xi 3. Added clarification that a 2x2 binary map aggregation based snow fraction will be implemented operationally for NPP in place of MESMA. on p xi. 4. Added reference to snow cover processing over Fresh Water lakes p xii. 5. Added description for Rev-A to section 1.4 Revsions on p. 2 6. Added reference to "inland water or coastal" to the third paragraph of section 2.4.1 titled Snow Binary Map on page 13 7. Added clarifications about snow fraction for NPP operations being based on 2x2 aggregation of the binary snow cover map in section 2.4.2 titled Snow Fraction" on p 14 8. Added description about snow cover code use of M15 and M16 in graceful degradation Brightness Temperatures for thermal screening p. 17 9. Added entry for moderate resolution brightness temperatures in table 6, on page 18 10 Added reference to M15 and M16 brightness temperature use on page 20. 11. Added that inland water and coastal pixels will be reported and quality flags set. and that AOT will be used for setting the aerosol exclusion quality flag on page 21 12. Added caveats for tables 7 & 8 instructing to refer to the most recent version of the Snow Cover OAD for parameter values and format. p22, 23 13. Added references to additional coastal and inland water quality flags implemented under SPCR 1131 on page 28 section 3.3.2 titled "Snow Quality and Weights" 14. Added description of binary map aggregated snow fraction in section 3.3.4 titled "Mathematical Description of the Snow Fraction Algorithm" p 33-34. 15. Added equations on p32-33 for lower and upper NSDI thresholds.	ii, xi, xii, p2, 13, 14, 17, 18, 20, 21, 22, 23, 28, 33-34,

D43758, B. PDMO Released: 2010-06-22 (VERIFY REVISION STATUS)
PDMO

Revision/Change Record

Document Number D43758

Revision	Document Date	Revision/Change Description	Pages Affected
B	02/17/2010	Revision B updates, reference ECR A-266A.	
		1. Changed Space Technology to Aerospace Systems, updated the Revision designation to Rev B.	Cover page
		2. Updated revision designation from Rev A to Rev B in document headers for all pages.	All
		3. Added missing equation numbers 3.3.3.2, 3.3.3.3 and 3.3.3.4 on pages 32 and 33	p 32-33
		4. Corrected band index numbers in the NDSI equation on page 31 and NDVI equation on page 32	p 31-32
		5. Deleted statement regarding setting quality weights to 0 for sun glint pixels consistent with changes made under SPCR 924 in Oct. 2005	p 31
		6. Deleted legacy MESMA algorithm statement about use of VIIRS M9 band to screen thin cirrus pixels. Added correct description of how the VIIRS algorithm uses the thin cirrus flag from the VCM IP to flag thin cirrus pixels	p 32
		7. Corrected corrupted fonts for the Greek letter Mu used in a sentence on page 53.	p 53
		8. Eliminated text, figures, table and sections related to the MESMA snow fraction algorithm	All
		9. Added reference to the Snow Cover OAD and CDFCB Volume 8	p1; 2
		Approved for Public Release per Contracts Letter 100610-02.	

D43758, B. PDMO Released: 2010-06-22 (VERIFY REVISION STATUS)
PDMO

TABLE OF CONTENTS

Page

LIST OF FIGURES iv

LIST OF TABLES v

GLOSSARY OF ACRONYMS vi

ABSTRACT ix

1.0 INTRODUCTION 1
- 1.1 PURPOSE 1
- 1.2 SCOPE 1
- 1.3 VIIRS DOCUMENTS 1
- 1.4 REVISIONS 2

2.0 EXPERIMENT OVERVIEW 4
- 2.1 OBJECTIVES OF THE SNOW COVER RETRIEVAL 4
- 2.2 INSTRUMENT CHARACTERISTICS 6
- 2.3 ALGORITHM HERITAGE 9
  - 2.3.1 NOAA/TIROS 9
  - 2.3.2 DMSP 9
  - 2.3.3 LANDSAT 10
  - 2.3.4 NASA/EOS 10
- 2.4 RETRIEVAL STRATEGY 10
  - 2.4.1 Snow Binary Map 10
  - 2.4.2 Snow Fraction 11
  - 2.4.3 Snow Depth 11
  - 2.4.4 Snow Albedo 12

3.0 ALGORITHM DESCRIPTION 13
- 3.1 PROCESSING OUTLINE 13
- 3.2 ALGORITHM INPUT 15
  - 3.2.1 VIIRS Data 15
- 3.3 THEORETICAL DESCRIPTION OF THE RETRIEVAL 17

D43758, B. PDMO Released: 2010-06-22 (VERIFY REVISION STATUS)
PDMO

3.3.1 Physics of the Problem 18
3.3.2 Snow Quality and Snow Weights 20
3.3.3 Mathematical Description of the Snow Binary Map Algorithm 23
3.3.4 Mathematical Description of the Snow Fraction Algorithm 26
3.3.5 Archived Algorithm Output 26

4.0 EDR PERFORMANCE 26
4.1 STRATIFICATION 26
4.1.1 Snow Binary Map 26
4.1.2 Snow Fraction 27
4.2 STRATIFIED PERFORMANCE ANALYSIS 27
4.2.1. Snow Binary Map 27
4.2.2 Snow Fraction 42
4.3 LIMITS OF APPLICABILITY 43
4.3.1 Cloudy 43
4.3.2 Low Light or Nighttime 43
4.3.3 Forest canopy (snow fraction) 44
4.4 PRACTICAL CONSIDERATIONS 44
4.4.1 Numerical Computation Considerations 44
4.4.2 Programming and Procedural Considerations 44
4.4.3 Configuration of Retrievals 45
4.4.4 Quality Assessment and Diagnostics 45
4.4.5 Exception Handling 45
4.5 VALIDATION 45

5.0 ASSUMPTIONS 49

6.0 REFERENCES 49

D43758, B. PDMO Released: 2010-06-22 (VERIFY REVISION STATUS)
PDMO

LIST OF FIGURES

Page

Figure 1. Summary of VIIRS design concepts and heritage. 7

Figure 2. VIIRS detector footprint aggregation scheme for building Imagery “pixels”. 8

Figure 3. Horizontal Sampling Interval (HSI) for imagery bands 8

Figure 4. Process flow for the Snow Cover EDR algorithm. 13

Figure 5: Representative reflectance spectra for snow, vegetation, soil, and water.....19

Figure 6: Representative reflectance spectra for snow and clouds 19

Figure 7: Near-Infrared Reflectance versus NDSI plot for winter and summer scenes...23

Figure 8: NDSI versus NDVI plot for modeled aspen, jack pine, and spruce stands.....24

Figure 9: Reflectance images of Death Valley scene (MAS/SUCCESS campaign).....29

Figure 10: NDSI versus NDVI scatter plot of the MAS Death Valley scene 30

Figure 11: Reflectance images of Brazil scene from MAS/SCAR-B campaign 31

Figure 12: NDSI versus NDVI scatter plot of the MAS Brazil scene (SCAR-B_163_1). .32

Figure 13. Reflectance images of Minnesota winter scene.....33

Figure 14: NDSI versus NDVI scatter plot of the MAS Minnesota winter scene.....34

Figure 15. MAS Images of Eastern Colorado obtained on February 13, 1997.....35

Figure 16: NDSI versus NDVI scatter plot of the MAS Colorado winter scene.....36

Figure 17: NDSI versus NDVI scatter plot the MAS Colorado winter scene 37

Figure 18: Probability of Correct Typing vs. Snow Fraction 38

Figure 19: MODIS (top) and Unit Test (bottom) Snow Binary Map.....42

Figure 20. Northern hemisphere snow cover classification from Sturm et al. (1995) 47

D43758, B. PDMO Released: 2010-06-22 (VERIFY REVISION STATUS)
PDMO

LIST OF TABLES

Page

Table 1. Specification of the NPOESS Snow Cover/Depth EDR 4

Table 2. Snow Binary Map Algorithm – Input Data Summary 9

Table 3. VIIRS Data for the VIIRS Snow Cover Algorithms 15

Table 4. Snow Binary Map Probability of Correct Typing (%).....38

Table 5. Error Budget for Retrieval of the Snow Binary Map EDR (Case 1).....39

Table 6. Error Budget for Retrieval of the Snow Binary Map EDR (Case 2).....40

Table 7. Error Budget for Retrieval of the Snow Binary Map EDR (Case 3).....40

Table 8. Categories of snow cover and climate parameters.....46

D43758, B. PDMO Released: 2010-06-22 (VERIFY REVISION STATUS)
PDMO

GLOSSARY OF ACRONYMS

AOT	Aerosol Optical Thickness
AMSR	Advanced Microwave Scanning Radiometer
ATBD	Algorithm Theoretical Basis Document
atm	Atmosphere
AVHRR	Advanced Very High Resolution Radiometer
AVIRIS	Airborne Visible/Infrared Imaging Spectrometer
AWS	Automatic Weather Station
BRDF	Bidirectional Reflectance Distribution Function
BRF	Bidirectional Reflectance Function
CDR	Critical Design Review
cm	Centimeters
CMIS	Conical Scanning Microwave Imager/Sounder
COT	Cloud Optical Thickness
DAAC	Distributed Active Archive Center
DISORT	Discrete Ordinates Radiative Transfer
DMSP	Defense Meteorological Satellite Program
DoD	Department of Defense
EDR	Environmental Data Record
ENVI	Environment for Visualizing Images
EOS	Earth Observing System
GC-NET	Greenland Climate Network
GCM	General Circulation Model
GIFOV	Ground Instantaneous Field of View
GLI	Global Imager
GSD	Ground Sample Distance
HCS	Horizontal Cell Size
HDF	Hierarchical Data Format
HSI	Horizontal Sampling Interval
HSR	Horizontal Spatial Resolution
IDPS	Interface Data Processing Segment
IP	Intermediate Product
IPW	Image Processing Workbench
LLLS	Low-Level Light Sensor
LSR	Li-Sparse Reciprocal

D43758, B. PDMO Released: 2010-06-22 (VERIFY REVISION STATUS)
PDMO

LUT	Look-Up Table
MAS	MODIS Airborne Simulator
MESMA	Multiple Endmember Spectral Mixture Analysis
MODIS	Moderate Resolution Imaging Spectroradiometer
MSS	Multispectral Scanner
MTF	Modulation Transfer Function
NASA	National Aeronautics and Space Administration
NASA/GSFC	NASA/Goddard Space Flight Center
NCEP	National Centers for Environmental Prediction
NDSI	Normalized Difference Snow Index
NDVI	Normalized Difference Vegetation Index
NESDIS	National Environmental Satellite, Data and Information Service
NGST	Northrop Grumman Space Technology
NIR	Near Infrared
NOAA	National Oceanic and Atmospheric Administration
NOHRSC	National Operational Hydrologic Remote Sensing Center
NPOESS	National Polar-orbiting Operational Environmental Satellite System
NPP	NPOESS Preparatory Program
OLS	Operational Linescan System
P^3I	Pre-Planned Product Improvement
PDR	Preliminary Design Review
RDR	Raw Data Record
RMS	Root Mean Square
RT	Radiative Transfer (also Ross Thick)
SBRS	Santa Barbara Remote Sensing
SCAR-B	Smoke, Clouds, and Radiation - Brazil
SDR	Sensor Data Record
SDSM	Solar Diffuser Stability Monitor
SMA	Spectral Mixture Analysis
SNR	Signal to Noise Ratio
SRD	Sensor Requirements Document
SRF	Spectral Response Function
SSM/I	Special System Microwave/Imager
SSPR	Shared System Performance Responsibility
SUCCESS	Subsonic Aircraft Contrail and Cloud Effects Special Study
SWE	Snow-Water Equivalent
SWIR	Short Wave Infrared

D43758, B. PDMO Released: 2010-06-22 (VERIFY REVISION STATUS)
PDMO

SZA	Solar Zenith Angle
TBD	To Be Determined
TBR	To Be Reviewed
THEMIS	Thermal Emission Imaging System
TIROS	Television Infrared Observing System
TM	Thematic Mapper
TOA	Top-of-Atmosphere
UCSB	University of California – Santa Barbara
UV	Ultraviolet
VIIRS	Visible/Infrared Imager/Radiometer Suite
VIS	Visible
VIS/IR	Visible/Infrared
VOAT	VIIRS Operational Algorithm Team
WINCE	Winter Cloud Experiment

D43758, B. PDMO Released: 2010-06-22 (VERIFY REVISION STATUS)
PDMO

ABSTRACT

The following document is Revision A of the Algorithm Theoretical Basis Document (ATBD) for snow cover retrieval from Top-of-Atmosphere (TOA) reflectances received by the National Polar-orbiting Operational Environmental Satellite System (NPOESS) Visible/Infrared Imager/Radiometer Suite (VIIRS). Snow Cover, a VIIRS level 2 product, is one of the required VIIRS Environmental Data Records (EDR) products for the NPOESS Snow Cover/Depth EDR, as stated in the NPOESS System Specification [SY15-0007]. The TOA reflectance will be supplied as a VIIRS Sensor Data Record (SDR), as documented in the VIIRS Radiometric Calibration ATBD *[Y3261]* D43777. The purpose of this document is to describe the theoretical basis and development process of the algorithms to retrieve a snow/no snow binary map and the fraction of snow cover in a specified horizontal cell, as required by the NPOESS System Specification.

A VIIRS Snow Cover EDR requirement is that a snow/no snow binary map be produced at a horizontal cell size of 0.5 km at nadir under clear, daytime conditions, with a probability of correct typing of 90% or better. The algorithm to retrieve the binary map uses the TOA reflectance in three VIIRS imagery resolution reflectance bands. It is an adaptation of the Moderate Resolution Imaging Spectroradiometer (MODIS) snow algorithm, which classifies a pixel as snow or no snow from its values of Normalized Difference Snow Index (NDSI) and Normalized Difference Vegetation Index (NDVI). The VIIRS algorithm uses a red band in place of the green band used by the MODIS algorithm, allowing us to achieve imagery resolution (0.4 km at nadir). Our analysis shows that the red band NDSI threshold is nearly identical to the green band NDSI threshold. Our performance analysis leads to a performance estimate of approximately 92% or better probability of correct typing for most cases, consistent with the performance of the MODIS algorithm. The algorithm, which will benefit directly from MODIS heritage, is a low risk approach with the capability of providing an operational, global snow cover product.

Another VIIRS Snow Cover EDR requirement is that snow fraction be retrieved globally at a horizontal cell size of 1.3 km under clear, daytime conditions. The measurement range will be the fraction of snow cover from 0 to 1, with a measurement uncertainty of 0.1. A Multiple Endmember Spectral Mixture Analysis (MESMA) algorithm was initially developed to retrieve snow fraction using the TOA reflectance in nine VIIRS moderate resolution reflectance bands to meet the specification measurement. Initial performance analysis indicated that the measurement uncertainty requirement potentially would not be achieved with the non-heritage MESMA algorithm. The MESMA based snow fraction has therefore not been implemented operationally. The operational algorithm implemented to retrieve snow fraction is based on a 2x2 aggregation of the VIIRS imagery resolution binary snow map. The uncertainty of the snow fraction product is therefore determined by the probability of correct typing performance associated with the snow binary map.

This document presents the algorithm theoretical basis, the input data requirements, the EDR performance specification and error analysis, conditions under which the specification cannot be attained, and the plan for initialization and validation.

D43758, B. PDMO Released: 2010-06-22 (VERIFY REVISION STATUS)
PDMO

1.0 INTRODUCTION

1.1 PURPOSE

This Algorithm Theoretical Basis Document (ATBD) explains the mathematical background to derive a snow/no snow binary map and snow fraction from Visible and Infrared top-of-atmosphere (TOA) reflectance. This document also provides an overview of required input data, physical theory, assumptions, limitations, and a performance analysis of the described algorithms. The retrieved snow products are part of the National Polar-orbiting, Operational Environmental Satellite System (NPOESS) Snow Cover/Depth Environmental Data Record (EDR). The TOA reflectances used for the retrieval are obtained from measurements of the Visible/Infrared Imager/Radiometer Suite (VIIRS) Sensor Data Record (SDR).

1.2 SCOPE

This document covers the theoretical basis for the derivation of the VIIRS Snow Cover EDR products, which consist of a snow/no snow binary map and snow fraction in a horizontal cell. The purpose and scope of the document are described in Section 1, while Section 2 provides an overview of the snow cover retrieval objectives. Section 3 describes the algorithm, its input data, the theoretical background, and some practical considerations. Section 4 contains the EDR performance analysis and error budget. Section 5 contains the pre-launch and post-launch plan for verification and validation. Section 6 contains assumptions and limitations.

1.3 VIIRS DOCUMENTS

This document contains references to other Raytheon VIIRS documents, designated by a document number, which is given in italicized brackets. The VIIRS documents cited in this document are:

[SY15-0007] - NPOESS System Specification (Rev N – September 12, 2008)

[PS 154640-101] - VIIRS Sensor Specification

D43313 - VIIRS Aerosol Optical Thickness and Particle Size Parameter ATBD (reference Y2388]

D43750 - VIIRS Cloud Optical Properties ATBD (reference Y2393]

D43755 - VIIRS Surface Albedo ATBD (reference Y2398]

D43759 - VIIRS Surface Type ATBD (reference Y2402]

D43765 - VIIRS Surface Reflectance ATBD (reference Y2411]

D43766 - VIIRS Cloud Mask ATBD, (reference Y2412]

D39592 – Operational Algorithm Description Document for the VIIRS Snow Cover Environmental Data Record (EDR)

D34862-08 – NPOESS Common Data Format Control Book – External Volume VIII –Look Up Table Formats

D43758, B. PDMO Released: 2010-06-22 (VERIFY REVISION STATUS)
PDMO

[Y2468] - VIIRS Operations Concept document

[Y2469] - VIIRS Context Level Software Architecture

[Y2470] - VIIRS Interface Control Document

[Y2471] - VIIRS Cloud Mask Detailed Design Document

[Y2472] - VIIRS Cloud Module-Level Software Architecture

[Y2477] - VIIRS Snow Ice Module Level Software Architecture

[Y2483] - VIIRS Surface Albedo Unit Level Detailed Design Document

[Y2498] - VIIRS Surface Reflectance Unit Level Detailed Design Document

[Y3234] - VIIRS Snow Cover Unit Level Detailed Design Document

[Y3236] - VIIRS Algorithm Design Verification Plan

[Y3237] - VIIRS Algorithm Software Integration and Test Plan

D43776 - VIIRS Geolocation ATBD [reference Y3258]

D43777 - VIIRS Radiometric Calibration ATBD [reference Y3261]

[Y3270] - VIIRS System Verification and Validation Plan

D43778 - VIIRS Earth Gridding ATBD [reference Y7051]

1.4 REVISIONS

Revision B of this document implements correction of typographical errors in the document prior to public release. The corrections also include updating information in tables VIIRS System Specification, removal of detailed formatting information related to tunable parameter tables that are described in the Operational Algorithm Description Document and removal of references to the MESMA snow fraction algorithm. Revision A of this document reflects algorithm development to allow processing over fresh water lakes (inland water and coastal pixels) and is a revision to the initial PCIM release (D43758) to bring the ATBD into Matrix accountability. The initial PCIM release (D43758) is equivalent to Raytheon document Y2401 dated April 21, 2005. That version was the fourth revision of version 5 of the VIIRS Snow Cover ATBD, dated April 21, 2005 and incorporates minor corrections for document header dates and typographical errors. The third revision of version 5 of the VIIRS Snow Cover ATBD, dated March 24, 2005 incorporated optional processing of snow cover fraction from the binary mask. The second revision reflects algorithm development performed under the VIIRS Algorithm Continuance SOW. The first revision of version 5, dated April 2002 was a minor revision of version 5.0, which was released in March 2002 as part of the Raytheon NPOESS/VIIRS Critical Design Review (CDR) package. The first two versions were developed in response to VIIRS Sensor Requirements Document (SRD), revision 1, dated August 3, 1998. The first version was dated October 1998. The second version was dated June 1999. The third version, dated May 2000, was developed in response to VIIRS Sensor Requirements Document (SRD), Version 2, Revision a, dated 04 November 1999 and was submitted as part of the Raytheon NPOESS/VIIRS Preliminary Design Review (PDR) and Proposal packages.

D43758, B. PDMO Released: 2010-06-22 (VERIFY REVISION STATUS)
PDMO

The primary purpose of version 4 was to respond to VIIRS Algorithm Watch List items generated by the VIIRS Operational Algorithm Team (VOAT). An additional purpose was to incorporate minor revisions generated by an internal Raytheon review since the VIIRS PDR. Changes since version 3 included:

- Inclusion of Bidirectional Reflectance Distribution Function (BRDF) correction factors
- Expanded description of input data, including VIIRS gridded data
- Revision and enhancement of the process flow description
- Responses to relevant VOAT Watch List Items and other reviewer comments

Version 5 incorporated the post-PDR developments in software architecture and detailed design that bring the algorithm to a CDR level of maturity. Changes since version 4 included:

- Additional development of the algorithm, with a detailed process flow and description of the LUTs.
- The introduction of a process that performs pixel masking and pixel weighting

Version 5, revision 2 was developed in the NPOESS EMD phase as part of the VIIRS Algorithm Continuance work, under the direction of the NPOESS Shared System Performance Responsibility (SSPR) contractor, Northrop Grumman Space Technology (NGST). Changes include:

- The addition of a thermal mask to the binary map algorithm. This change brings the binary map algorithm closer to MODIS heritage.
- The development and expansion of modeled snow reflectance in the Snow Reflectance LUTs. In the previous version, a single LUT contained surface reflectance models for three snow types, derived from MODTRAN 4.0. In the revised version, there are separate LUTs for each of 9 moderate resolution bands, each of 24 snow types, and two aerosol models. The LUTs contain BRDF-corrected TOA reflectance derived from DISORT and 6S.
- The use of TOA reflectance instead of surface reflectance as input data. This change brings the binary map algorithm closer to MODIS heritage and also corresponds to the changes in the Snow Reflectance LUT.
- A new approach for non-snow reflectance estimation in the snow fraction algorithm. The new approach replaces modeled non-snow BRDF with an empirical kernel-based BRDF, and adopts the atmospheric correction of the VIIRS Surface Reflectance algorithm to estimate non-snow TOA reflectance instead of non-snow surface reflectance.
- Addition of a capability to model snow TOA reflectance in cases of rough terrain.

D43758, B. PDMO Released: 2010-06-22 (VERIFY REVISION STATUS)
PDMO

2.0 EXPERIMENT OVERVIEW

2.1 OBJECTIVES OF THE SNOW COVER RETRIEVAL

Because of its high albedo, snow is an important factor in determining the radiation balance, with implications for global climate studies (Foster and Chang, 1993). General circulation models (GCM) do not simulate the Arctic climate very well (Bromwich and Tzeng, 1994), indicating the need to improve measurements of the global snow cover. Weekly snow cover maps of the Northern Hemisphere have been produced since 1966 by the National Oceanic and Atmospheric Administration (NOAA: Matson, Roeplewski, and Varnadore, 1986; Matson, 1991). Daily and 8-day composite global maps are an objective of the recently launched National Aeronautics and Space Administration (NASA) Moderate Resolution Imaging Spectroradiometer (MODIS) instrument (Hall et al., 1998). Regionally, the measurement of snowpack properties is vital to the prediction of water supply and flood potential (Carroll *et al.,* 1989; Chang *et al.,* 1987). Regional snow products with 1 km resolution are produced by the National Weather Service (Carroll, 1990), and at 500 meter resolution from MODIS **http://modis-snow-ice.gsfc.nasa.gov/snow.html.** The objective of the VIIRS retrieval is to achieve the performance specifications designed to meet the requirements stated in the NPOESS System Specification. These are listed in Table 1.

Table 1. Specification of the NPOESS Snow Cover/Depth EDR

Paragraph	Subject	Specified Value
	a. Horizontal Cell Size	
40.6.3-1a	1. Nadir	0.8 km
40.6.3-1b	2.Edge of Swath	1.6 km
40.6.3-3a	b. Horizontal Reporting Interval	HCS
40.6.3-4	c. Snow Depth Ranges	Snow/No Snow
40.6.3-5	d. Horizontal Coverage	Land
40.6.3-7	f. Measurement Range	0 - 100% of HCS
40.6.3-8	g. Measurement Uncertainty	10% of HCS (Snow/No Snow)
40.6.3-10	h. Mapping Uncertainty, 3 Sigma	1.5 km
40.6.3-12	i. Max Local Average Revisit Time	24 hrs Daytime Only
	j. Binary HCS	
40.6.3-14a	1. Nadir	0.4 km
40.6.3-14b	2. Edge Of Swath	0.8 km
40.6.3-16	l. Long Term Stability (C)	10%
40.6.3-17	m. Latency	NPP - 140 min. NPOESS - 28 min.
40.6.3-18	n. Binary Map- Measurement Range	Snow/No Snow
40.6.3-19	o. Binary Map- Probability of Correct Typing	90%
40.6.3-21	p. Measurement Uncertainty Degradation If Solar Zenith Angle 70 to 85 deg	40% of HCS (Snow/No Snow)
40.6.3-22	r. Measurement Exclusions:	

D43758, B. PDMO Released: 2010-06-22 (VERIFY REVISION STATUS)
PDMO

Paragraph	Subject	Specified Value
40.6.3-22a	1. Snow Fraction Measurement Exclusion Condition: Horizontal Cell Contains Forest Canopy	
40.6.3-22b	2. Binary Map Probability of Correct Typing Exclusion Condition: Snow Fraction 0.2 to 0.7 or Solar Zenith Angle > 60 deg	
40.6.3-22c	3. All Measurements If Aerosol Optical Thickness > 1.0	
40.6.3-22d	4. All Measurements If Solar Zenith Angle > 85 deg	

Paragraph	Subject	Specified Value
	a. Horizontal Cell Size	
40.6.3-1a	1. Nadir	0.8 km
40.6.3-1b	2.Edge of Swath	1.6 km
40.6.3-3a	b. Horizontal Reporting Interval	HCS
40.6.3-4	c. Snow Depth Ranges	Snow/No Snow
40.6.3-5	d. Horizontal Coverage	Land
40.6.3-7	f. Measurement Range	0 - 100% of HCS
40.6.3-8	g. Measurement Uncertainty	10% of HCS (Snow/No Snow)
40.6.3-10	h. Mapping Uncertainty, 3 Sigma	1.5 km
40.6.3-12	i. Max Local Average Revisit Time	24 hrs Daytime Only
	j. Binary HCS	
40.6.3-14a	1. Nadir	0.4 km
40.6.3-14b	2. Edge Of Swath	0.8 km
40.6.3-16	l. Long Term Stability (C)	10%
40.6.3-17	m. Latency	NPP - 140 min. NPOESS - 28 min.
40.6.3-18	n. Binary Map- Measurement Range	Snow/No Snow
40.6.3-19	o. Binary Map- Probability of Correct Typing	90%
40.6.3-21	p. Measurement Uncertainty Degradation If Solar Zenith Angle 70 to 85 deg	40% of HCS (Snow/No Snow)
40.6.3-22	r. Measurement Exclusions:	
40.6.3-22a	1. Snow Fraction Measurement Exclusion Condition: Horizontal Cell Contains Forest Canopy	
40.6.3-22b	2. Binary Map Probability of Correct Typing Exclusion Condition: Snow Fraction 0.2 to 0.7 or Solar Zenith Angle > 60 deg	
40.6.3-22c	3. All Measurements If Aerosol Optical Thickness > 1.0	
40.6.3-22d	4. All Measurements If Solar Zenith Angle > 85 deg	

[1] NPOESS System Specification *[SY 15-0007, Rev. N]*

The specifications apply under clear, daytime conditions only. Surface properties cannot be observed through cloud cover by a Visible/Infrared (VIS/IR) sensor.

D43758, B. PDMO Released: 2010-06-22 (VERIFY REVISION STATUS)
PDMO

2.2 INSTRUMENT CHARACTERISTICS

The VIIRS instrument can be pictured as a convergence of three existing sensors.

The Operational Linescan System (OLS) is the operational visible/infrared scanner for the Department of Defense (DoD). Its unique strengths are controlled growth in spatial resolution through rotation of the ground instantaneous field of view (GIFOV) and the existence of a low-level light sensor (LLLS) capable of detecting visible radiation at night. OLS has primarily served as a data source for manual analysis of imagery. The Advanced Very High Resolution Radiometer (AVHRR) is the operational visible/infrared sensor flown on the National Oceanic and Atmospheric Administration (NOAA) Television Infrared Observation Satellite (TIROS-N) series of satellites (Planet, 1988). Its unique strengths are low operational and production cost and the presence of five spectral channels that can be used in a wide number of combinations to produce operational and research products. In December 1999, the National Aeronautics and Space Administration (NASA) launched the Earth Observing System (EOS) morning satellite, *Terra*, which includes the Moderate Resolution Imaging Spectroradiometer (MODIS). This sensor possesses an unprecedented array of thirty-two spectral bands at resolutions ranging from 250 m to 1 km at nadir, allowing for unparalleled accuracy in a wide range of satellite-based environmental measurements. A second MODIS sensor was included on the EOS afternoon satellite *Aqua*, launched May 4, 2002.

VIIRS will reside on a platform of the National Polar-orbiting Operational Environmental Satellite System (NPOESS) series of satellites. It is intended to be the product of a convergence between DoD, NOAA and NASA in the form of a single visible/infrared sensor capable of satisfying the needs of all three communities, as well as the research community beyond. As such, VIIRS will require three key attributes: high spatial resolution with controlled growth off nadir, minimal production and operational cost, and a large number of spectral bands to satisfy the requirements for generating accurate operational and scientific products.

The VIIRS sensor specification is based on the sensor requirements of the National Polar-orbiting Operational Environmental Satellite System (NPOESS) and on EDR thresholds and objectives. The Snow Cover algorithm takes as input geolocated, calibrated Sensor Data Records (SDRs) generated from three VIIRS Imagery bands and nine VIIRS moderate resolution bands. The SDRs are obtained from VIIRS RDRs by an RDR to SDR process. The RDRs are obtained by a rotating telescope scanning mechanism that minimizes the effects of solar impingement and scattered light. Figure 1 illustrates the design concept for VIIRS, designed and built by Raytheon Santa Barbara Remote Sensing (SBRS). VIIRS is essentially a combination of SeaWiFS foreoptics and an all-reflective modification of MODIS/THEMIS aft-optics. Calibration is performed onboard using a solar diffuser for short wavelengths and a blackbody source and deep space view for thermal wavelengths. A solar diffuser stability monitor (SDSM) is also included to track the performance of the solar diffuser. The VIIRS scan will extend to 56 degrees on either side of nadir, providing a swath of 3000 km for the nominal satellite altitude of 833 km.

D43758, B. PDMO Released: 2010-06-22 (VERIFY REVISION STATUS)
PDMO

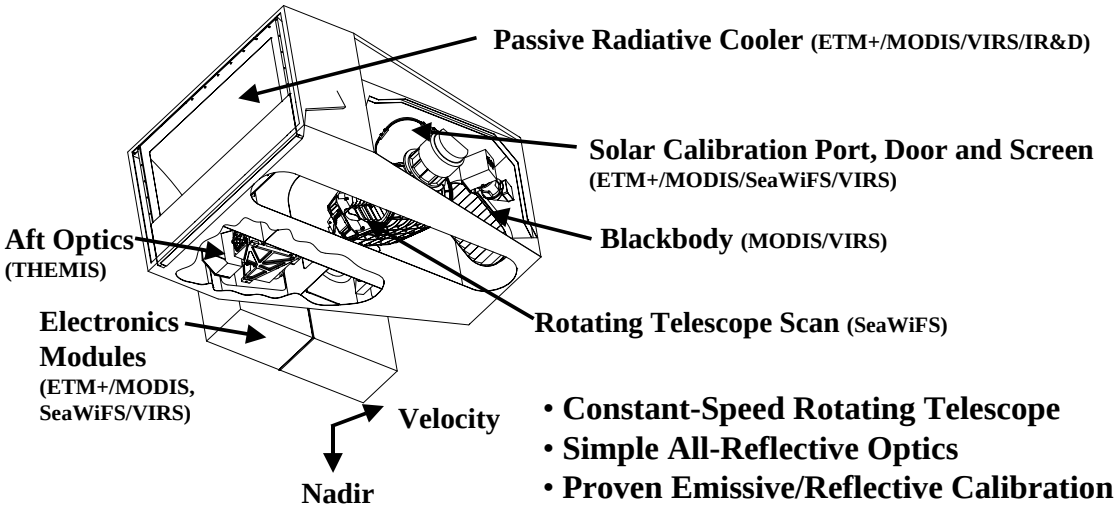

Figure 1. Summary of VIIRS design concepts and heritage.

The VIIRS Sensor Requirements Document (SRD) placed explicit requirements on spatial resolution for the VIIRS sensor. Specifically, the horizontal spatial resolution (HSR) of bands used to meet threshold Imagery EDR requirements must be no greater than 400 m at nadir and 800 m at the edge of the scan. This led to the development of a unique scanning approach which optimizes both spatial resolution and signal to noise ratio (SNR) across the scan. The concept is summarized in Figure 2 for the imagery (fine resolution) bands. The VIIRS detectors are rectangular, with the smaller dimension along the scan. At nadir, three detector footprints are aggregated to form a single VIIRS “pixel.” Moving along the scan away from nadir, the detector footprints become larger both along track and along scan, due to geometric effects and the curvature of the Earth. The effects are much larger along scan. At 31.59 degrees in scan angle, the aggregation scheme is changed from 3x1 to 2x1. A similar switch from 2x1 to 1x1 aggregation occurs at 44.68 degrees. The VIIRS scan consequently exhibits a pixel growth factor of only 2 both along track and along scan, compared with a growth factor of 6 along scan which would be realized without the use of the aggregation scheme. This scanning approach allows VIIRS to provide imagery at 800-m resolution or finer globally, with 375-m resolution at nadir. Additionally, due to the imagery requirements for VIIRS and the “sliver” detector design, MTF performance will be extremely sharp (0.5 at Nyquist).

D43758, B. PDMO Released: 2010-06-22 (VERIFY REVISION STATUS)
PDMO

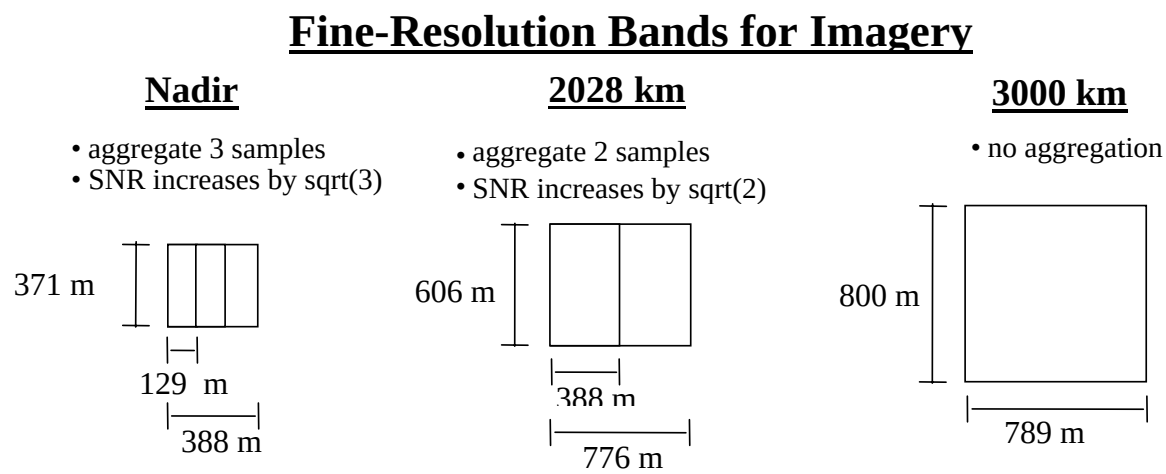

Figure 2. VIIRS detector footprint aggregation scheme for building Imagery "pixels".

Figure 3, showing the Horizontal Sampling Interval (HSI) that results from the combination scan/aggregation scheme, illustrates the benefits of the aggregation scheme for spatial resolution.

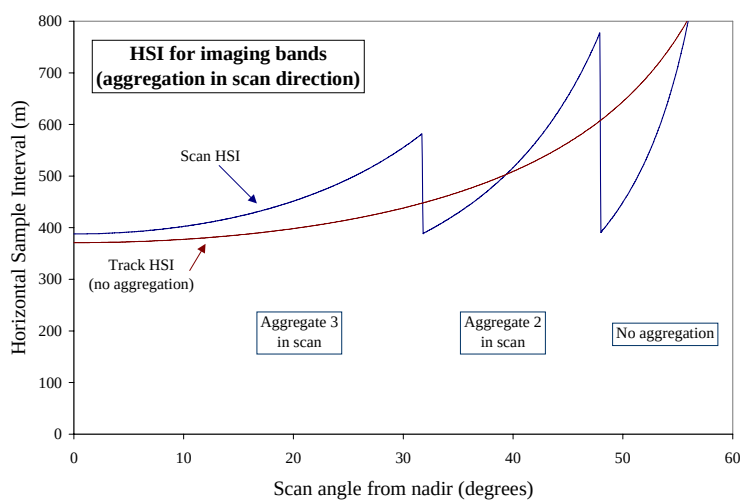

Figure 3. Horizontal Sampling Interval (HSI) for imagery bands (aggregation in scan direction).

The aggregation switch points occur at scan angles of 31.59 degrees (3 to 2 aggregation) and 44.68 degrees (2 to no aggregation).

The performance characteristics of the bands used by the Snow Cover algorithm, listed in Table 1 and Table 2, are obtained from the VIIRS Sensor Specification Document *[PS 154640-101]* and the VIIRS Radiometric Calibration ATBD *[Y3261].* The VIIRS sensor has been designed from the NPOESS sensor requirements and the flowdown of EDR requirements. Complete details on the instrument design are provided in the Raytheon VIIRS Sensor Specification Document *[PS154640-101]*.

D43758, B. PDMO Released: 2010-06-22 (VERIFY REVISION STATUS)
PDMO

The binary map algorithm uses TOA reflectance in three bands at imagery resolution and brightness temperature in one band at imagery resolution. Table 2 lists the characteristics of these bands.

Table 2. Snow Binary Map Algorithm – Input Data Summary

VIIRS Band	λ(μm)	Δλ(μm)	GSD[1] (m) at Nadir (Track x Scan)	HCS[2] (m) at Nadir (Track x Scan)	GSD (m) at Edge of Scan (Track x Scan)	HCS (m) at Edge of Scan (Track x Scan)
I1	0.640	0.080	371 x 131	371 x 393	800 x 800	800 x 800
I2	0.865	0.039	371 x 131	371 x 393	800 x 800	800 x 800
I3	1.61	0.060	371 x 131	371 x 392	800 x 800	800 x 800
I5	11.45	1.9	371 x 131	371 x 392	800 x 800	800 x 800

[1] - Ground Sample Distance [2] - Horizontal Cell Size

2.3 ALGORITHM HERITAGE

2.3.1 NOAA/TIROS

Initially, the weekly NOAA National Environmental Satellite Data and Information System (NESDIS) operational product was determined from visible satellite imagery from polar-orbiting and geostationary satellites and surface observations. The analysis was performed once a week, using the most recent clear view of the surface. Because the analysis for this product was done only once a week, much snow cover, especially from fleeting/transient storms, was missed. Where cloud cover precluded the analyst's view of the surface for an entire week, the analysis from the previous week was carried forward (Ramsay, 1998). The maps were hand drawn, and then digitized using an 89 X 89 line grid overlaid on a stereographic map of the Northern Hemisphere. In 1997, the older, weekly maps were replaced in 1997, by the IMS product. The IMS product provides a daily snow map that is constructed through the use of a combination of techniques including visible, near-infrared and passive-microwave imagery and meteorological-station data at a spatial resolution of about 25 km (Ramsay, 1998 and 2000).

Regional snow products, with 1-km resolution, are produced operationally in 3000 - 4000 drainage basins in North America by the National Weather Service using NOAA National Operational Hydrologic Remote Sensing Center (NOHRSC) data (Carroll, 1990 and Rango, 1993).

2.3.2 DMSP

Passive-microwave sensors on-board the Nimbus 5, 6, and 7 satellites and the Defense Meteorological Satellite Program (DMSP) have been used successfully for measuring snow extent at

D43758, B. PDMO Released: 2010-06-22 (VERIFY REVISION STATUS)
PDMO

a 25- to 30-km resolution through cloud-cover and darkness since 1978 (Chang et al., 1987). Passive-microwave sensors also provide information on global snow depth (Foster et al., 1984).

2.3.3 LANDSAT

The LANDSAT Multispectral Scanner (MSS) and TM sensors, with 80-m and 30-m resolution, respectively, are useful for measurement of snow covered area over drainage basins (Rango and Martinec, 1982). Additionally, LANDSAT TM data are useful for the quantitative measurement of snow reflectance (Dozier et al., 1981; Dozier, 1984 and 1989; Hall et al., 1989; Winther, 1992).

2.3.4 NASA/EOS

The launch of the EOS Terra and Aqua satellites introduced a new era in global snow mapping. The MODIS snow products (**http://modis-snow-ice.gsfc.nasa.gov/snow.html**) include daily and 8-day composites of global snow cover at 500-m resolution. Statistics will be provided regarding the extent and persistence of snow cover at each grid cell for the Level-3 products. These products are produced from the MODIS Level-2 snow product, which is a swath-based snow/no snow binary map, derived by the MODIS snow-mapping algorithm (Snowmap; Hall et al., 1998, 2001a). Our binary map algorithm, discussed in Section 3, draws heavily from the MODIS algorithm, and in fact is designed to continue MODIS heritage as faithfully as possible.

Advanced Microwave Scanning Radiometer (AMSR)-derived snow and ice maps are also available from the EOS Aqua and Terra satellites. It is envisioned that a product can be developed that will employ reflective and passive-microwave data that will permit snow extent, albedo and depth to be mapped, thus enabling daily maps to be generated irrespective of cloud cover and darkness. The MODIS/AMSR data will be very useful in the development of a prospective NPOESS pre-planned product improvement (P^3I) for snow cover/depth, using VIIRS/CMIS data.

2.4 RETRIEVAL STRATEGY

2.4.1 Snow Binary Map

The input data will consist of a two-dimensional grid of surface pixels for each of three VIIRS imagery resolution bands in the form of geolocated TOA reflectance, supplied by the VIIRS EV_375M SDR.

The Cloud Mask algorithm *[Y2412]* will identify pixels that should be excluded from processing due to cloud or cloud shadow. The Cloud Mask will also supply a land/water mask.

Each pixel will be examined for its suitability. Pixels designated as land, inland water or coastal by the land/water mask and as “clear” or “probably clear” by the cloud mask will be passed for processing. Pixels designated as “probably clear, inland water or coastal” will have a quality flag attached to them. The solar/sensor angles for each pixel will be used to determine whether the pixel is rejected, passed for further processing with a quality flag attached, or passed for further processing without reservation.

D43758, B. PDMO Released: 2010-06-22 (VERIFY REVISION STATUS)
PDMO

Pixels which have been passed for processing will have their values of NDSI, NDVI, Visible and NIR reflectance examined to determine a snow or no snow classification, following the prescription described in Section 3.3.2.

Recent MODIS experience suggests that a thermal mask should be used to avoid snow classification from dense forest regions in the tropics (Barton, Hall, and Riggs 2001). Application of a threshold 11 micron brightness temperature of 283K screens out all pixels with greater surface temperature. The VIIRS algorithm adopts the same brightness temperature threshold and applies it to the VIIRS 11.45 micron (I5) band brightness temperature obtained from the VIIRS EV_375M SDR.

The process flow to implement the snow binary map retrieval is outlined in Section 3.1.

2.4.2 Snow Fraction

The input data for the snow cover fraction will consist of the binary snow cover map which will be aggregated to a fraction using a 2x2 aggregation of the imagery resolution snow binary map. Snow fraction computed using 2x2 aggregation of the binary snow mask, results in reporting of snow fraction in 25% increments.

The Cloud Mask algorithm *[Y2412]* will identify pixels that should be excluded from processing due to cloud and will also supply a land/water mask. The VIIRS Cloud Mask IP *[Y2471]* is expected to supply a forest mask to identify boreal forest pixels requiring special consideration.

Each pixel will be examined for its suitability. A pixel weighting process is followed, using a Snow Quality LUT to assign pixel weights according to band, various atmospheric conditions, and various surface conditions (c.f. Section 3.3.2). Pixels designated as land by the land/water mask and as clear or probably clear by the cloud mask will be passed for processing. Pixels designated as “forest” by the forest mask will have a quality flag attached to them. Pixels designated as “probably clear” or “thin cirrus” will be given a reduced pixel weight, and will have a quality flag attached to them. The solar/sensor angles, aerosol optical thickness, and cloud optical thickness (COT mode only) for each pixel will be used to derive pixel quality and pixel weight for each band. These will determine whether the pixel is rejected, passed for further processing with a quality flag attached, or passed for further processing without reservation.

The process flow to implement snow fraction retrieval is outlined in Section 3.1

2.4.3 Snow Depth

Snow depth is not a VIIRS requirement. It is recognized that data fusion between high resolution snow cover from VIS/IR and snow depth at coarser resolution from passive microwave would improve the overall snow product. MODIS/AMSR studies can be used to investigate this possibility, and could serve as a precursor to an NPOESS Level 3 P^3I product. For the purposes of our algorithm development, however, we are required to produce a VIIRS Snow Cover EDR product within an operational timeline that precludes the use of contemporaneous CMIS data. We have therefore deferred a consideration of a combined VIIRS/CMIS snow cover/depth product.

D43758, B. PDMO Released: 2010-06-22 (VERIFY REVISION STATUS)
PDMO

2.4.4 Snow Albedo

A snow albedo algorithm has been developed for MODIS (Klein 2001; Klein, Hall, and Nolin, 2001), but will not be implemented in the VIIRS snow algorithm for two reasons:

1) Snow albedo is not a required Snow Cover/Depth EDR product.

2) The VIIRS Surface Albedo EDR will produce surface albedo over all land surfaces, including surfaces with snow cover *[Y2398].*

D43758, B. PDMO Released: 2010-06-22 (VERIFY REVISION STATUS)
PDMO

3.0 ALGORITHM DESCRIPTION

3.1 PROCESSING OUTLINE

The VIIRS Snow Cover EDR is retrieved by an automated algorithm. The process flow is implemented within the Snow/Ice Module by the independent testable Snow Cover software unit, as illustrated in Figure 4.

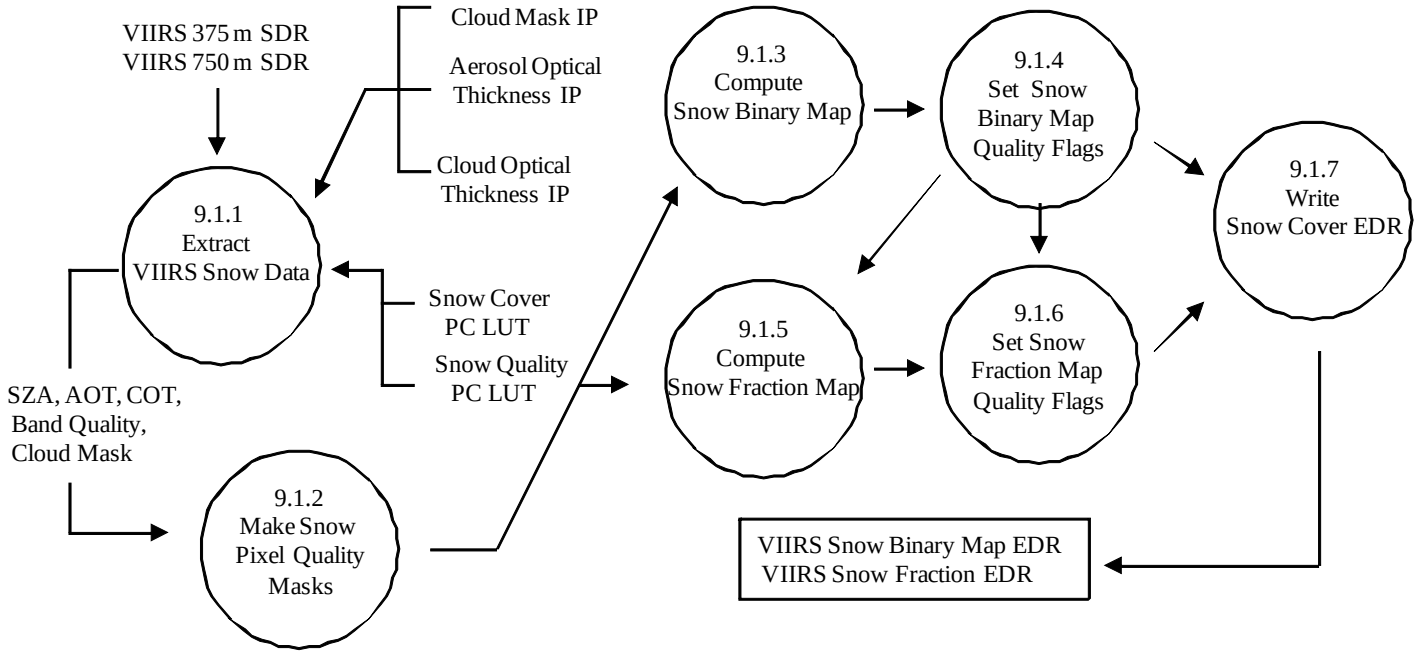

Figure 4. Process flow for the Snow Cover EDR algorithm.

The process flow is described in detail in the VIIRS Snow/Ice Module Level Software Architecture document *[Y2477]* and the Snow Cover Unit Level detailed design document *[Y3234]*. The main steps are as follows:

1) Input data for the current VIIRS granule is extracted by the *Extract VIIRS Snow Data* process. If all pixels are designated as Ocean in the Cloud Mask IP, processing is bypassed and a null EDR file is written.

2) The *Make Snow Pixel Masks* process (Section 3.3.2) performs pixel masking and pixel weighting, using information in the VIIRS EV_375M SDR *[Y3261]*, VIIRS Aerosol Optical Thickness IP *[Y2388]*, VIIRS Cloud Optical Thickness IP *[Y2472]*, VIIRS Cloud Mask IP

D43758, B. PDMO Released: 2010-06-22 (VERIFY REVISION STATUS)
PDMO

[Y2412], and a Snow Quality LUT *[Y3234].* The process produces a pixel quality mask and pixel weights for each band.

3) Observed TOA reflectance from VIIRS imagery resolution bands I1 (Visible), I2 (Near Infrared - NIR), and I3 (Short Wave Infrared - SWIR) are obtained from the VIIRS EV_375M SDR. Observed brightness temperature for the VIIRS I5 band is also obtained from the SDR. Bad pixels are identified from the Imagery Snow Mask, and the Imagery Band Weights. The *Compute Snow Binary Map* process calculates a snow/no snow binary map for each good imagery resolution pixel, using the snow binary map algorithm adapted from MODIS (Section 3.3.3).

4) Observed Brightness temperatures for the VIIRS M15 and M16 bands moderate resolution bands are obtained from the VIIRS EV_750M SDR *[Y3261]*. The moderate resolution brightness temperatures are utilized for screening of pixels with brightness temperatures exceeding 283 K in the event that the I5 band brightness temperature is bad quality.Bad pixels are identified from the Moderate Snow Mask, and the Moderate Band Weights.

5) The snow/no snow binary map for each imagery resolution pixel is written to the VIIRS Snow Cover EDR, along with associated pixel quality flags. The snow fraction for each moderate resolution pixel is also written to the EDR, along with associated pixel quality flags and pixel weights. The snow fraction pixel weight is the total of the individual band weights for that pixel, as determined by the *Make Snow Pixel Quality Masks* process.

D43758, B. PDMO Released: 2010-06-22 (VERIFY REVISION STATUS)
PDMO

3.2 ALGORITHM INPUT

3.2.1 VIIRS Data

The snow binary map and snow fraction algorithms require the VIIRS data listed in Table 3.

Table 3. VIIRS Data for the VIIRS Snow Cover Algorithms

Input Data	Source of Data	Reference
TOA Reflectance (I1, I2, I3)	EV_375M SDR [1]	*[Y3261]*
Brightness Temperature (I5)	EV_375M SDR [1]	*[Y3261]*
Brightness Temerature (M15, M16)	EV_750M SDR [1]	*[Y3261]*
Instrument Band Quality (I1, I2, I3, I5)	EV_375M SDR [1]	*[Y3261]*
Geodetic Coordinates	EV_375M SDR*, EV_750M SDR	*[Y3258]*
Solar/Sensor Angles	VIIRS SDR [1]	*[Y3258]*
Cloud Mask	VIIRS Cloud Mask IP [2]	*[Y2412]*
Land/Water Mask	VIIRS Cloud Mask IP [2]	*[Y2412]*
Forest Mask	VIIRS Cloud Mask IP [2]	*[Y2412]*
Aerosol Optical Thickness	Aerosol Optical Thickness IP [2]	*[Y2388]*
Cloud Optical Thickness	Cloud Optical Thickness IP [2]	*[Y2393]*
Snow Quality Parameters	Snow Quality LUT [3]	*[D34862-08]; [D39592]*
Snow Cover Parameters	Snow Cover LUT [3]	*[D34862-08] [D39592]*

[1] SDR = Sensor Data Record [2] IP = Intermediate Product [3] LUT= Look-up Table

TOA Reflectance

The VIIRS SDR will provide TOA reflectance for three imagery resolution bands (I1, I2, I3) used by the snow binary map algorithm.

Brightness Temperature

The VIIRS SDR will provide the I5, M15 and M16 band brightness temperatures used by the snow binary map algorithm. VIIRS M15 and M16 band data are used only as backup “graceful degradation” purposes.

D43758, B. PDMO Released: 2010-06-22 (VERIFY REVISION STATUS)
PDMO

Instrument Band Quality

The Build-SDR module will attach quality flags to the SDRs. The snow algorithm uses the SDR quality flags for each band to assign pixel weights. Pixels containing bad quality for I1, I2, or I3 will not be processed by the binary map algorithm.

Geodetic Coordinates

Pixel geodetic coordinates will be used to report the latitude/longitude coordinate to the EDR.

Solar / Sensor Angles

Pixels with solar zenith angle greater than 85 degrees will be excluded from further processing. The Pixels with solar zenith angle between 70 degrees and 85 degrees will be processed, but with a quality flag attached. The final setting of these values will be made as part of the initialization plan, and may depend upon aerosol optical thickness (AOT).

Cloud Mask

The VIIRS cloud mask *[Y2412]* is expected to derive a status of confident clear / probably clear / probably cloudy / confident cloudy for each pixel, building on MODIS cloud mask heritage (Ackerman *et al.*, 1997). Pixels classified as “confidently cloudy” will be excluded from further processing. Pixels classified as “probably clear” and probably cloudy will be processed. For these pixels, the pixel weight will be reduced by a factor obtained from the Snow Quality LUT, and a pixel quality flag will be written to the output EDR. Pixels classified as “confident clear” will be processed with no weight reduction. The cloud mask will also flag pixels that are shadowed by clouds. In that case, a cloud shadow weight reduction factor will be assigned to those pixels and a shadow quality flag will be written to the EDR. The cloud mask will also supply thin cirrus, sun glint, and active fire flags, which our algorithm will use to assign pixel weight and pixel quality to the data.

Land/Water Mask

The EDR will be reported for land pixels, inland water and coastal pixels. Ocean pixels pixels will be excluded from further processing by having their weight set to zero. Coastline pixel weights will be reduced to bad quality and reported with a quality flag. Inland water pixels will have their quality reduced to degraded (medium quality) and reported with a quality flag. Information on Land/Ocean/Inland Water/Coastline status will be obtained from the Cloud Mask IP *[Y2412]*, using the best quality land/water map available.

Forest Mask

A forest mask will be obtained from the Cloud Mask.. A forest canopy quality flag will be assigned to those pixels associated with the forest mask.

Aerosol Optical Thickness

D43758, B. PDMO Released: 2010-06-22 (VERIFY REVISION STATUS)
PDMO

Aerosol optical thickness (AOT) is obtained at moderate pixel resolution from the Aerosol Optical Thickness IP. It is used to derive pixel quality and pixel weight and to set the aerosol optical thickness exclusion quality flag for both the Snow Binary Map and 2x2 aggregated Snow Fraction algorithms.

Cloud Optical Thickness

Cloud optical thickness (COT) is obtained at moderate pixel resolution from the Cloud Optical Thickness IP. It can be used to derive pixel quality and pixel weight, as an alternative to the Cloud Mask. A switch in the Snow Quality LUT determines which alternative is used.

Snow Quality Parameters

The parameters in the Snow Quality LUT are used to determine quality for each pixel/band combination. They include a switch determining whether to use the Cloud Mask IP or the Cloud Optical Thickness IP for cloud masking, default relative weights for the nine moderate resolution bands, and weight reduction factors for various types of clouds, AOT, and solar zenith angle (SZA). The weight reduction factors in the current LUT are intended as an initial guess. It is expected that these will be refined during pre-launch verification and post-launch validation (c.f. Section 4.5). A detailed description of the LUT parameters can be found in the Snow Cover Operational Algorithm Description (OAD) document *[D39592]* and in the NPOESS Common Data Format Control Book *[D34862-08]*.

Snow Cover Parameters

A set of input parameters will be obtained from a pre-set VIIRS Snow Cover LUT. Refer to the most recent version of the Snow Cover OAD for updated parameter definitions, values and formats.
Tunable LUT parameters include an I5 Brightness temperature threshold, I1 and I2 reflectance thresholds, NDSI thresholds, and coefficients used to determine the allowed range of NDVI for a given value of NDSI (c.f. Figures 7 and 8). The values of these parameters have been initialized from MODIS experience (Klein, Hall, and Riggs (1998)) and will be tuned by validation activities (Section 4.5). These parameters direct the implementation of the algorithm (Section 3.3.2). A detailed description can be found in *[Y3234]* , the Snow Cover Operational Algorithm Description (OAD) document *[D39592]* and in the NPOESS Common Data Format Control Book *[D34862-08]*. .

3.3 THEORETICAL DESCRIPTION OF THE RETRIEVAL

The processes outlined in Section 3.1 only apply to regions that have successfully passed the quality examinations. Descriptions of the mathematical backgrounds of these processes follow.

D43758, B. PDMO Released: 2010-06-22 (VERIFY REVISION STATUS)
PDMO

3.3.1 Physics of the Problem

The reflectance of snow is unique among land cover types. It is among the brightest of natural substances in the visible and near-infrared part of the spectrum, but it is also often the darkest in the short wave infrared (Dozier, 1989). The spectral albedo of snow is wavelength-dependent, and this spectral dependency is controlled by the imaginary part *(k)* of the complex refractive index. This reaches a minimum at a wavelength of about 0.46 microns, and increases by a factor of 10^6 – 10^7 as wavelength increases out to 2.5 microns (Warren, 1982; Dozier, 1989).

Light in snow is scattered primarily by refraction through the ice grains. Nearly 89 percent is refracted through the grain, and 8 percent is scattered after internal reflections (Bohren and Barkstrom, 1974). Because ice is so transparent to visible radiation, snow reflectance is only weakly sensitive to grain size in bands below 0.7 microns, but sensitive to light absorbing impurities in the snow and, for optically-thin snowpacks, to snow water equivalent (SWE; Wiscombe and Warren, 1980; Grenfell, Perovich, and Ogren*,* 1981). Because light absorption by ice is much stronger in bands above 1.4 microns, reflectance at these wavelengths is relatively insensitive to absorbing impurities and SWE, but sensitive to changes in grain size, especially for grain radii less than 500 microns. Light absorbing particulates, such as dust and soot, affect snow reflectance out to 0.9 microns (Warren and Wiscombe, 1980), so the 0.86 micron band is sensitive to both absorbing impurities and grain size.

Clouds and snow are both bright across the visible and near-infrared region, but clouds are much brighter than snow in the short wave infrared (SWIR). This is because the smaller size of the scatterers in clouds decreases the probability of absorption in this spectral region where ice and water are moderately absorptive (Crane and Anderson, 1984; Dozier, 1984, 1989). Conversely, bodies of open water are dark at all wavelengths. Vegetation is dark in the visible bands because of absorption by photosynthetic pigments, but has a maximum reflectance between 0.7 and 1.3 microns. Because of leaf cell structure (Hoffer, 1978), SWIR reflectance is inversely related to leaf water content for healthy vegetation. Nevertheless, the reflectance at wavelengths longer than 1.5 microns is still high compared to that of snow. Most rock and soil spectra are the reverse of snow's. Absorption by iron oxides and organic matter strongly reduce visible reflectance, while those in the SWIR remain high.

Typical reflectance properties of snow and other surfaces are illustrated in Figure 5. An illustration of snow/cloud reflectance differences is in Figure 6.

D43758, B. PDMO Released: 2010-06-22 (VERIFY REVISION STATUS)
PDMO

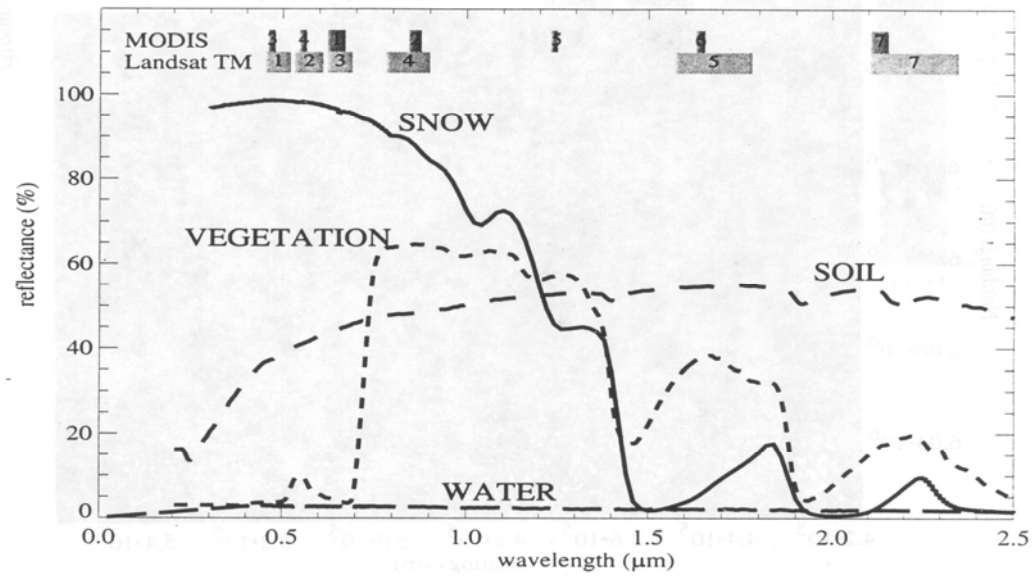

Figure 5: Representative reflectance spectra for snow, vegetation, soil, and water (from Klein, Hall, and Riggs, 1998).

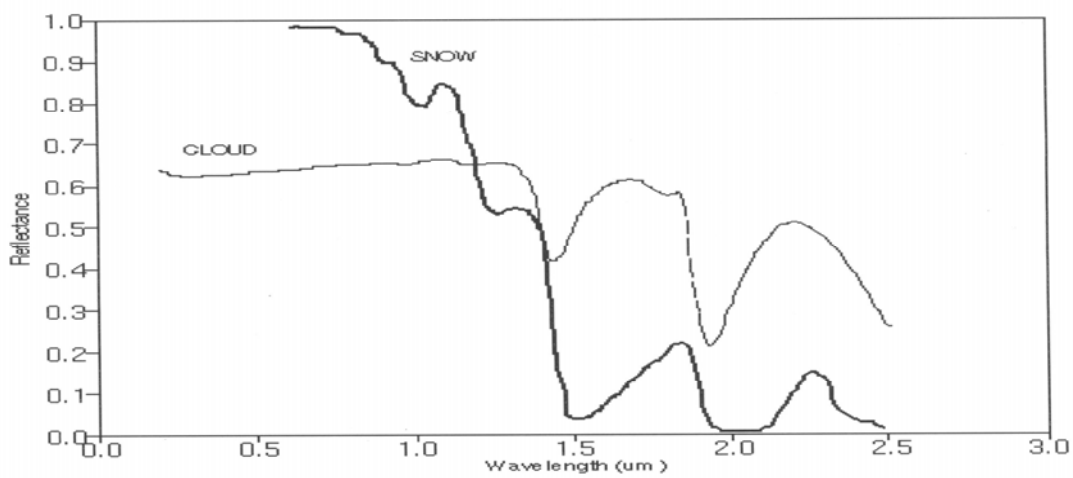

Figure 6: Representative reflectance spectra for snow and clouds (from Hall et al., 1998).

D43758, B. PDMO Released: 2010-06-22 (VERIFY REVISION STATUS)
PDMO

It is important to note that the reflectance spectra shown in the previous figures are representative of one specific case of snow type and cloud type. Real surfaces will exhibit spectral variability for any given surface type. In particular, snow reflectance depends on grain size and impurities. Cloud reflectance will vary with optical thickness, effective particle size, and phase.

The VIIRS Snow Cover EDR requirements apply to snow cover of any depth. Snow is such an efficient scatterer of visible and infrared radiation that the reflectance properties of snow are not very sensitive to snow depth or SWE. The physical basis for retrieval of snow depth or SWE is that the scattering efficiency of snow is measurably dependent on frequency in the passive microwave range of the spectrum. Microwave radiation upwelling from the underlying surface is scattered away from the sensor as it propagates through the snow pack. Thus, brightness temperatures at any given microwave frequency are lower for deeper snow packs. In addition, the scattering efficiency increases with frequency over the microwave range. As a result, differences in brightness temperatures at different microwave frequencies are correlated with the SWE. This physical principle is the basis for SWE retrieval algorithms based on passive microwave observations (Grody and Basist, 1996; Foster, Chang, Foster, and Hall, 1997; Chang, 1998).

3.3.2 Snow Quality and Snow Weights

The quality of the VIIRS Snow Cover EDR products will be degraded by the presence of clouds and aerosols in the path of the TOA radiance that is received at the sensor. Clouds and aerosols will have a varying effect, depending on optical thickness, type, and wavelength. Degradation will also occur due to effects of forest canopy, coastline, active fires, and sunglint. To account for these varying degradations, we determine weights for each pixel/band combination.

The *Make Snow Pixel Masks* process performs pixel masking and pixel weighting, using information in the VIIRS EV_375M SDR *[Y3261]*, VIIRS Aerosol Optical Thickness IP *[Y2388]*, VIIRS Cloud Optical Thickness IP *[Y2472]*, VIIRS Cloud Mask IP *[Y2412]*, and the Snow Quality LUT *[Y3234].* The process produces a pixel quality mask and pixel weights for each band.

Pixel quality flag masks are determined for both imagery resolution and moderate resolution pixels.

D43758, B. PDMO Released: 2010-06-22 (VERIFY REVISION STATUS)
PDMO

The “Land/Water” flags (coastal, inland water, ocean) are set if the VIIRS Cloud Mask IP *[Y2412]* indicates that the pixel is not fully land. The “Forest” flag is set if the VIIRS Cloud Mask IP indicates that the pixel contains forest canopy. The “Coastline” ” flag is set if the VIIRS Cloud Mask IP indicates that the pixel contains coastline. The “Cloud Quality” flag reproduces the Cloud Confidence bits of the VIIRS Cloud Mask IP. The “Thin Cirrus” flag reproduces the Thin Cirrus bits of the VIIRS Cloud Mask IP. The “Cloud Shadow” flag is set if the VIIRS Cloud Mask IP indicates that the pixel contains cloud shadow. The “Cloud Phase” flag reproduces the Cloud Phase bits of the VIIRS Cloud Mask IP. The “Fire” flag is set if the VIIRS Cloud Mask IP indicates that the pixel contains an active fire. The “Sunglint” ” flag is set if the VIIRS Cloud Mask IP indicates that the pixel is contaminated by sunglint.

The “Band Quality” flags are set if the VIIRS SDR indicates that the pixel contains bad data for that band.

The “Overall Quality” flag contains two bits for each band. These bits indicate “Green”, “Green/Yellow”, “Yellow/Red”, and “Red” quality. The algorithm assigns one of the four quality conditions to each (pixel, band) combination by determining weights. If the (pixel, band) weight is greater than the “Green” threshold value, a “Green” quality is assigned. If the (pixel, band) weight is less than the “Green” threshold value and greater than the “Yellow” threshold value, a “Green/Yellow” quality is assigned. If the (pixel, band) weight is less than the “Green/Yellow” threshold value and greater than the “Yellow/Red” threshold value, a “Yellow/Red” quality is assigned. Finally, if the (pixel, band) weight is less than the “Yellow/Red” threshold value, a “Red” quality is assigned.

The weights are obtained by reducing an initialized band weight (w_0) by various weight reduction factors:

$$w(\text{band, pixel}) = w_0(\text{band}) * w_1(\text{band, pixel}) * w_2(\text{band, pixel}) * \ldots * w_N(\text{band, pixel}) \qquad (3.3.2.1)$$

where w_N are the various weight reduction factors. These include Clouds, Aerosols, Active Fires, and Sunglint.

Clouds

Weight reduction factors for cloud contamination are obtained from the Snow Quality LUT. The LUT includes factors for various cloud types (water, ice, and mixed), thin cirrus, cloud shadow, and cloud adjacency. Information on cloud type for each moderate resolution pixel, obtained from the VIIRS Cloud Mask IP, includes Cloud Phase, Cloud Confidence (“Confident Clear”, “Probably Clear”, Probably Cloudy”, “Confident Cloudy”), Cloud Shadow, Cloud Adjacency, and Thin Cirrus. If the Cloud Confidence for a given pixel is “Probably Cloudy” or “Confident Cloudy”, the pixel weight is set to zero for all bands. If the Cloud Confidence for a given pixel is “Probably Clear”, we apply a cloud weight reduction factor. This factor depends on cloud type, which is obtained from the Cloud Phase information in the Cloud Mask IP. Separate weight reduction factors are applied for Thin Cirrus, Cloud Shadow, and Cloud Adjacency, if the Cloud Mask IP indicates that these conditions exist for a given pixel.

D43758, B. PDMO Released: 2010-06-22 (VERIFY REVISION STATUS)
PDMO

The algorithm allows for the option of determining cloud weight reduction factors from cloud optical thickness (COT), obtained from the VIIRS Cloud Optical Properties IP. This option is controlled by a switch in the Snow Quality LUT. The COT-dependent weight reduction factor is determined from the COT thresholds obtained from the Snow Quality LUT. These include “Red/Yellow” and “Yellow/Green” thresholds. If the pixel COT is greater than the “Red/Yellow” threshold for a given band, the pixel/band weight is set to zero. If the pixel COT is less than the “Yellow/Green” threshold for a given band, the pixel/band weight is unaffected. For a pixel COT in the range between the two thresholds, the pixel/band weight is reduced by a factor computed by linear interpolation of COT between the two thresholds:

$$w(band, pixel) = w(band, pixel) * w_{cloud} \quad (3.3.2.2)$$

where:

$$w_{cloud} = (COT_YR(band) – COT(pixel)) / (COY_YR(band) – COT_GY(band)) \quad (3.3.2.3)$$

Aerosols

Weight reduction factors for aerosols are determined in combination with the solar zenith angle (SZA), to allow for greater aerosol degradation at higher SZA. Band-dependent threshold values of SZA for a set of aerosol optical thickness (AOT) nodes are obtained from the Snow Quality LUT. These include “Red/Yellow” and “Yellow/Green” thresholds. If the pixel SZA is greater than the “Red/Yellow” threshold for a given band, the pixel/band weight is set to zero. If the pixel SZA is less than the “Yellow/Green” threshold for a given band, the pixel/band weight is unaffected. For a pixel SZA in the range between the two thresholds, the pixel/band weight is reduced by a factor computed by linear interpolation of SZA between the two thresholds:

$$w(band, pixel) = w(band, pixel) * w_{aerosol} \quad (3.3.2.4)$$

where:

$$w_{aerosol} = (SZA_YR(band) – SZA(pixel)) / (SZA_YR(band) – SZA_GY(band)) \quad (3.3.2.5)$$

Active Fires

If a given pixel has an indication of containing an active fire, the weight is set to zero for all bands. The Active Fires bit of the Cloud Mask IP is used to make this determination.

Sunglint

The Sunglint bits of the Cloud Mask IP are used to make this determination. A retrieval will still be performed for sunglint pixels.

D43758, B. PDMO Released: 2010-06-22 (VERIFY REVISION STATUS)
PDMO

3.3.3 Mathematical Description of the Snow Binary Map Algorithm

The algorithm is an adaptation of the binary classification technique of the MODIS algorithm, SNOMAP (Hall *et al.,* 1998). SNOMAP classifies snow by a Normalized Difference Snow Index (NDSI) of 0.555 μm and 1.64 μm bands and additional reflectance thresholds. Our algorithm is an adaptation of the MODIS algorithm. We use an NDSI from the 0.64 μm and 1.61 μm VIIRS imagery resolution bands, combined with reflectance thresholds in the 0.865 μm and 0.64 μm VIIRS imagery resolution bands, to classify a VIIRS pixel as snow or non-snow at imagery resolution.

$$NDSI = (R_1 - R_3) / (R_1 + R_3) \qquad (3.3.3.1)$$

Where: R_1, R_3 = TOA reflectance in 0.64 μm (I1), 1.61 μm (I3) VIIRS bands

Pixels with an NDSI > 0.4 and a 0.865 μm (I2 band) TOA reflectance > 0.11 are classified as snow. These thresholds have been developed from pre-launch MODIS characterization, as described in the MODIS ATBD (Hall *et al.,* 1998). The application of these thresholds is shown as Figure 7.

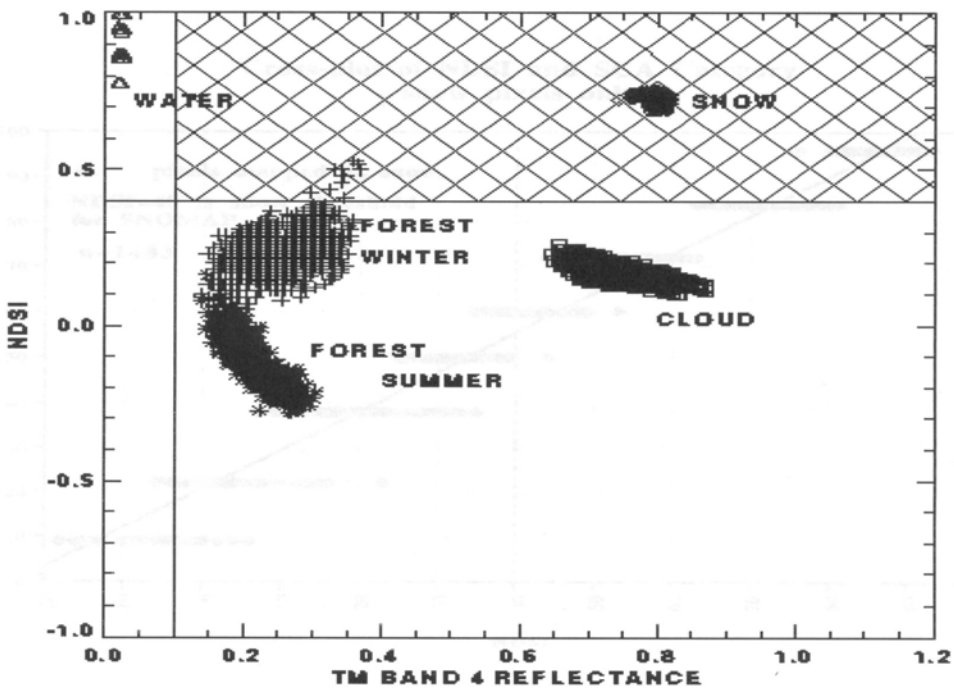

Figure 7: Near-Infrared Reflectance versus NDSI plot for winter and summer scenes (Landsat TM scenes of Glacier National Park, Montana (from Hall et al., 1998)).

Pixels located in the cross-hatched region of Figure 7 are classified as snow. Winter forest pixels, which are known to have snow cover under the forest canopy, are incorrectly classified as no snow.

While the NDSI can separate snow from most obscuring clouds, it does not always identify or discriminate optically-thin cirrus clouds from snow. We will follow the MODIS approach (Hall et al.,

D43758, B. PDMO Released: 2010-06-22 (VERIFY REVISION STATUS)
PDMO

2001a) by using the thin cirrus quality flag provided by the VIIRS Cloud Mask IP to flag thin cirrus pixels.

The VIIRS algorithm, following MODIS algorithm heritage, also uses a Normalized Difference Vegetation Index (NDVI) to classify snow covered forest pixels by location in an NDSI/NDVI scatter plot.

$$NDVI = (R_2 - R_1) / (R_1 + R_2) \qquad (3.3.3.2)$$

Where: R_1, R_2 = TOA reflectance in 0.64 μm (I1), 0.865 μm (I2) VIIRS bands

Pixels with 0.1 < NDSI < 0.4 are classified as snow cover under a forest canopy, if NDVI is greater than a threshold value. The threshold depends on the pixel NDSI. These thresholds have been developed from pre-launch MODIS characterization. A snow reflectance model was used in conjunction with a canopy reflectance model (GeoSAIL) to develop the thresholds, which were then tested on Landsat TM images of the southern BOREAS study area in Prince Albert National Park, Saskatchewan. Details can be found in Klein, Hall, and Riggs (1998). The application of these thresholds is shown as Figure 8.

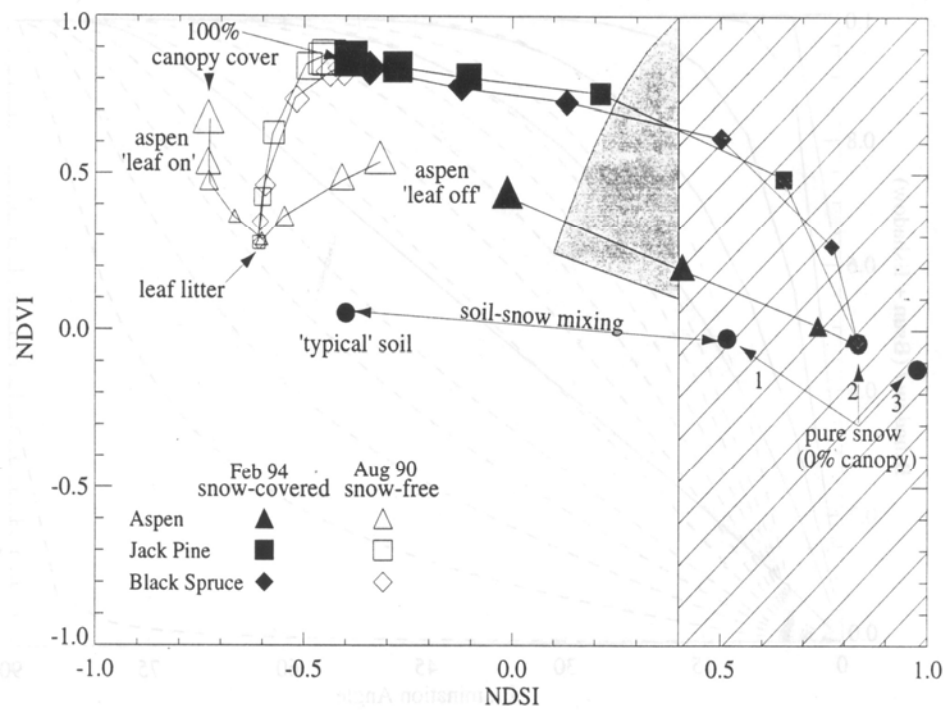

Figure 8: NDSI versus NDVI plot for modeled aspen, jack pine, and spruce stands (from Klein, Hall, and Riggs, 1998).

The hatched region in Figure 8 is the snow classification region for the Version 4 MODIS algorithm. The gray shaded region represents a proposed additional region for capturing snow-covered forests. Our algorithm also adopts this approach. The lower and upper NDVI thresholds in figure 8 are related to NDSI according to the following equations:

D43758, B. PDMO Released: 2010-06-22 (VERIFY REVISION STATUS)
PDMO

$$\text{ndvi_range}(1) = \alpha(1) + \alpha(2) * \text{NDSI} \quad (3.3.3.3)$$

$$\text{ndvi_range}(2) = \beta(1) + \beta(2) * \text{NDSI} + \beta(3) * \text{NDSI}^2 + \beta(4) * \text{NDSI}^3 \quad (3.3.3.4)$$

The expression for ndvi_range(1) represents the lower NDVI threshold which is linearly related to NDSI. The coefficients $\alpha(1)$ and $\alpha(2)$ are defined as tunable parameters. The expression for ndvi_range(2) represents the upper, non-linear NDVI threshold. The coefficients $\beta(1)$, $\beta(2)$, $\beta3)$ and $\beta(4)$ are also defined as tunable parameters. The above relationships are applied for cloud free pixels with NDSI between 0.1 and 0.4 and brightness temperature below 283 K.

One of the problems facing the MODIS snow-mapping algorithm is the mapping of snow in regions where it is known not to exist. One of the more common locations for this problem is in dark, dense forests, particularly in the tropics. The nature of the snow-mapping algorithm is such that it is particularly sensitive to small changes in the NDSI or NDVI over dark, dense vegetation.

To correct false-snow mappings in tropical forests, the 11.03 µm thermal-infrared band (MODIS band 31) is used to estimate the surface temperature. This band was selected because it represents an atmospheric window, in which little of the emitted thermal radiation is absorbed by the atmosphere. A tentative threshold of 277 K was set. When this threshold is applied in tropical regions, e.g., the Congo, it eliminates from 93% to 98% of the false snow (Barton, Hall, and Riggs 2001). More recently, this threshold has been revised to 283K. The VIIRS snow algorithm adapts the MODIS thermal mask, using the VIIRS I5 band (11.45 µm) brightness temperature as the nearest imagery resolution equivalent to MODIS band 31.

The accuracy of the MODIS snow maps varies with land-cover type (Hall et al., 2001a). This is not surprising, since a single NDSI threshold is applied to surfaces with a variety of characteristic NDSI values. Our algorithm will have the benefit of access to a global surface type database (the VIIRS Surface Type-Biomes IP *[Y2402]*). It is therefore possible to develop and apply surface-type dependent NDSI thresholds, with the potential of improving performance. Implementation of surface-type dependent thresholds is not included in the current version of the VIIRS snow algorithm, as it is our primary interest to maintain MODIS heritage prior to NPP launch, but is recommended as a future product improvement.

MODIS validation has shown a weak relationship between scan angle and the presence of false snow, with more false snow mapped at higher scan angles (Hall et al., 2001a). Numerical tests show that from 35% to 60% of the snow detection in a given scene can be found at scan angles greater than 45°. Statistically, most of this must be false snow detection. It is also observed in the data that almost all of the false snow is mapped on the sunward side of the sensor. This phenomenon is probably due to forward scattering off of various atmospheric or ground-level agents. It is expected that BRDF correction of the observed VIIRS TOA reflectance would mitigate most of this effect. BRDF correction factors could be developed from the same radiative transfer models that estimate snow TOA reflectance for the snow fraction algorithm (c.f. Section 3.3.4.2). Implementation of a BRDF correction is not included in the current version of the VIIRS snow binary map algorithm, as it is our

D43758, B. PDMO Released: 2010-06-22 (VERIFY REVISION STATUS)
PDMO

primary interest to maintain MODIS heritage prior to NPP launch, but is recommended as a future product improvement.

3.3.4 Mathematical Description of the Snow Fraction Algorithm

Snow cover fraction is based on a 2x2 aggregation of the VIIRS imagery resolution snow binary map pixels to yield a moderate resolution snow fraction with measurement uncertainty of 0.25. The aggregation scheme utilizes a 2x2 pixel imagery resolution window. The aggregated snow cover fractions may take on values of 0, 0.25, 0.50, 0.75 or 1.0 or fill.

3.3.5 Archived Algorithm Output

Algorithm output will be written to the VIIRS Snow Cover EDR, in HDF EOS format. The binary snow map will be archived at imagery pixel resolution as a yes/no bit for each pixel, along with associated pixel quality flags. The retrieved fraction of snow for each VIIRS pixel will be archived at moderate pixel resolution, along with the derived snow type, associated pixel quality flags and snow fraction pixel weights.

4.0 EDR PERFORMANCE

The performance of the algorithms with respect to the VIIRS requirements and the System Specification (c.f. Tables 1, 2, and 3) is reviewed in this section.

EDR performance shall be verified by analysis, modeling, and/or simulation based on the instrument design and performance characteristics and the algorithms. The analysis, modeling, and/or simulation shall be sufficiently extensive in scope to verify that EDR requirements are met under a broad range of conditions that are representative of those occurring in nature, include typical and extreme conditions.

4.1 STRATIFICATION

4.1.1 Snow Binary Map

We identify the following stratifications for the snow binary map:

i. Snow fraction “truth”

ii. Sensor view angle

iii. Solar zenith angle

iv. Fraction of mixed pixels

D43758, B. PDMO Released: 2010-06-22 (VERIFY REVISION STATUS)
PDMO

Performance of the snow binary map algorithm will depend on snow fraction. The probability of correct typing for any binary classifier must approach 50% as the threshold for defining yes/no “truth” is approached. Our algorithm thresholds have been tuned to a threshold of 0.5 in snow fraction. That is, the probability of correct typing will increase as true fraction differs from 0.5. A sensible stratification must then include snow fraction “truth” as a parameter. We have selected 5 ranges of snow fraction, 0.0-0.2, 0.2-0.4, 0.4-0.6, 0.6-0.8, and 0.8-1.0. We have deliberately selected these ranges so that they are symmetric with respect to 0.5, where we expect minimum EDR performance.

The requirements are specified at nadir. Our stratification of sensor view angle is restricted to nadir view.

We have used a solar zenith angle of 60 degrees in our simulations to date. Our stratification of solar zenith angle is restricted to this value. A wider range of solar zenith angles will be simulated in the future.

It is informative to report EDR performance for a representative range of structured scenes. We parameterize this range as a stratification by fraction of mixed pixels in a scene. Scenes with a greater fraction of mixed pixels are expected to have a reduced EDR performance because spatial errors (MTF, band misregistration) are greater. We have selected three stratifications by fraction of mixed pixels, 10% (easy), 30% (typical), and 50% (hard).

4.1.2 Snow Fraction

The performance of snow fraction is determined by the performance of the snow binary map since the snow fraction is based on a 2x2 aggregation of the snow binary map pixels.

4.2 STRATIFIED PERFORMANCE ANALYSIS

4.2.1. Snow Binary Map

4.2.1.1 Pre-CDR

Performance verification prior to the Critical Design Review was by demonstration.

We classified MODIS Airborne Simulator (MAS) scenes as snow or no snow at a 50 meter pixel resolution, with the aid of an unsupervised 6 band classification in ENVI. Manual review of the ENVI classifications was performed to assign each ENVI-derived class as snow or no snow.

We aggregated each scene to pixel sizes of 0.4 km and 0.8 km to simulate VIIRS pixels at nadir and edge of scan respectively. We classified each VIIRS pixel as snow or no snow, depending upon the number of snow/no snow MAS pixels in the aggregate. At nadir, a VIIRS pixel is an aggregate of 64 MAS pixels. For a VIIRS nadir pixel to be classified as snow, it required 33 or more MAS pixels classified as snow. For a VIIRS nadir pixel to be classified as no snow, it required 33 or more MAS pixels classified as no snow. These classifications are used as “VIIRS truth”.

D43758, B. PDMO Released: 2010-06-22 (VERIFY REVISION STATUS)
PDMO

A number of perturbations were applied to the scenes to simulate sensor/algorithm performance.

Reflectance errors were applied to the scenes. We perturbed the aggregated reflectance in MAS bands 3 (648 nm), 7 (866 nm), and 10 (1.63 μm), using model errors for the Surface Reflectance IP in VIIRS bands I1 (640 nm), I2 (865 nm), and I3 (1.61 μm). We have obtained these from the performance analysis of the Surface Reflectance algorithm *[Y2411]*. Reflectance accuracy errors were modeled by assuming an aerosol optical thickness (AOT) of 0.1 and a 0.05 offset between true AOT and the AOT acquired from a climatological database. Details on the creation and use of the aerosol climatology are found in the Aerosol Optical Thickness and Particle Size Parameter ATBD *[Y2388]*. Our selection of AOT mean and offset is based on studies of typical aerosol conditions in the sub-arctic (Blanchet and List, 1983). Reflectance precision errors were modeled from the sensor noise performance specification. The reflectance errors depend on surface reflectance truth, which is correlated with snow fraction. Reflectance errors were calculated for a solar zenith angle of 60 degrees.

Spatial errors were also applied to the scene. The scenes were perturbed by MTF smearing, following the sensor MTF performance specification. Band misregistration was simulated by offsetting the NIR and SWIR bands by 0.2 pixels with respect to the visible band, consistent with the VIIRS sensor specification for band registration *[PS154640-101]*.

We applied the algorithm to the perturbed VIIRS scenes to retrieve snow/no snow, and computed probability of correct typing by comparing the retrieved classifications to the “VIIRS truth”. We did this for four scenes:

i. A Death Valley scene containing no snow cover (SUCCESS_115_16)

ii. A Brazil scene containing no snow cover (SCAR-B_163_1)

iii. A Northern Minnesota scene containing 100% snow cover under a varying canopy (WINCE_49_06)

iv. A mixed snow/no snow scene in Colorado in February (WINCE_50_14)

The first two scenes test the algorithm performance over desert and vegetated non-snow surfaces. The third scene tests the performance in winter forest regions. The fourth scene tests the performance for a typical case of mixed snow/no snow pixels.

Death Valley Scene: Visible (.645 μm) and SWIR (1.6μm) images of the scene are shown in Figure 9. There is of course no snow in the scene. The bright feature is a salt pan. It can not be distinguished from snow by the visible data alone (Figure 11a), but its brightness in the SWIR (Figure 9b) does distingueish it from snow.

D43758, B. PDMO Released: 2010-06-22 (VERIFY REVISION STATUS)
PDMO

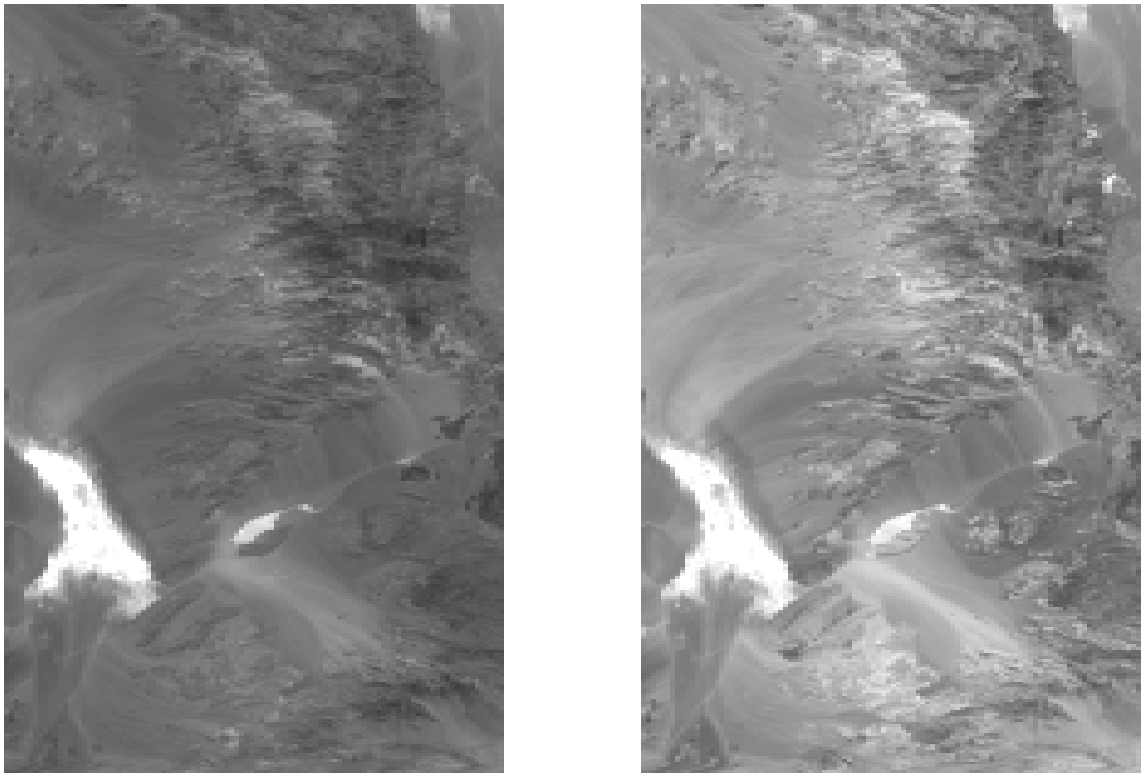

(a) **(b)**

Figure 9: Reflectance images of Death Valley scene (MAS/SUCCESS campaign) ((a) Visible reflectance, (b) Short Wave IR reflectance)

The range of the gray scale for Figure 9 is from 0.0 to 0.5 in reflectance.

D43758, B. PDMO Released: 2010-06-22 (VERIFY REVISION STATUS)
PDMO

The NDSI/NDVI scatter plot for the Death Valley scene is shown in Figure 10. Expected system performance errors were added to the scenes.

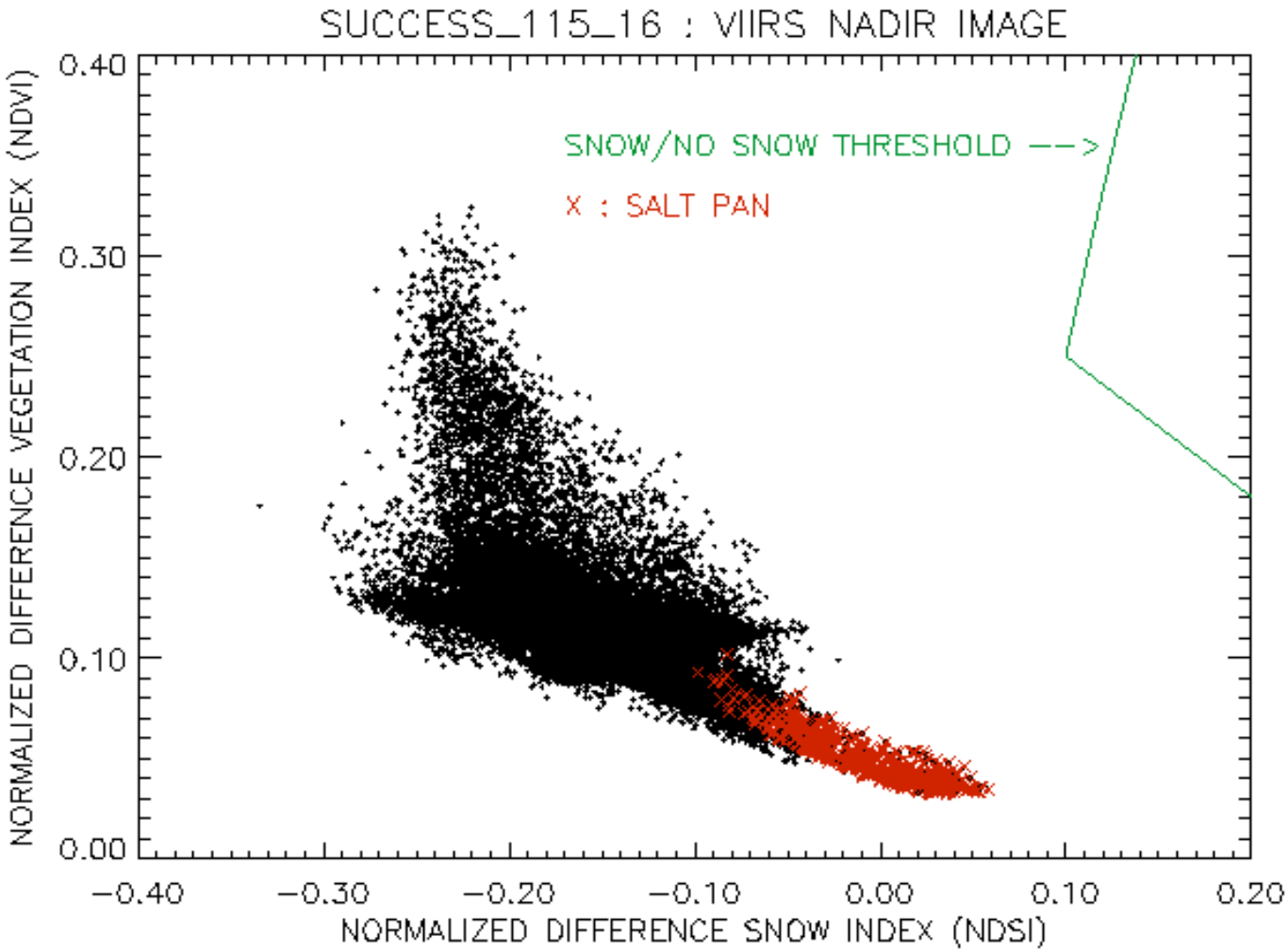

Figure 10: NDSI versus NDVI scatter plot of the MAS Death Valley scene (SUCCESS_115_16).

Each data point in the Figure 10 scatter plot represents a VIIRS pixel at nadir, obtained by aggregating the MAS pixels to a VIIRS nadir pixel size. Correct classification occurs when pixels classified as snow fall to the right of the green threshold boundary and when pixels classified as no snow fall to the left of the boundary. All pixels in this scene were correctly classified as no snow, including the salt pan.

D43758, B. PDMO Released: 2010-06-22 (VERIFY REVISION STATUS)
PDMO

Brazil Scene: Visible (.645 μm) reflectance, NDVI, and NDSI images of the scene are shown in Figure 11. There is of course no snow in the scene.

(a) **(b)** **(c)**

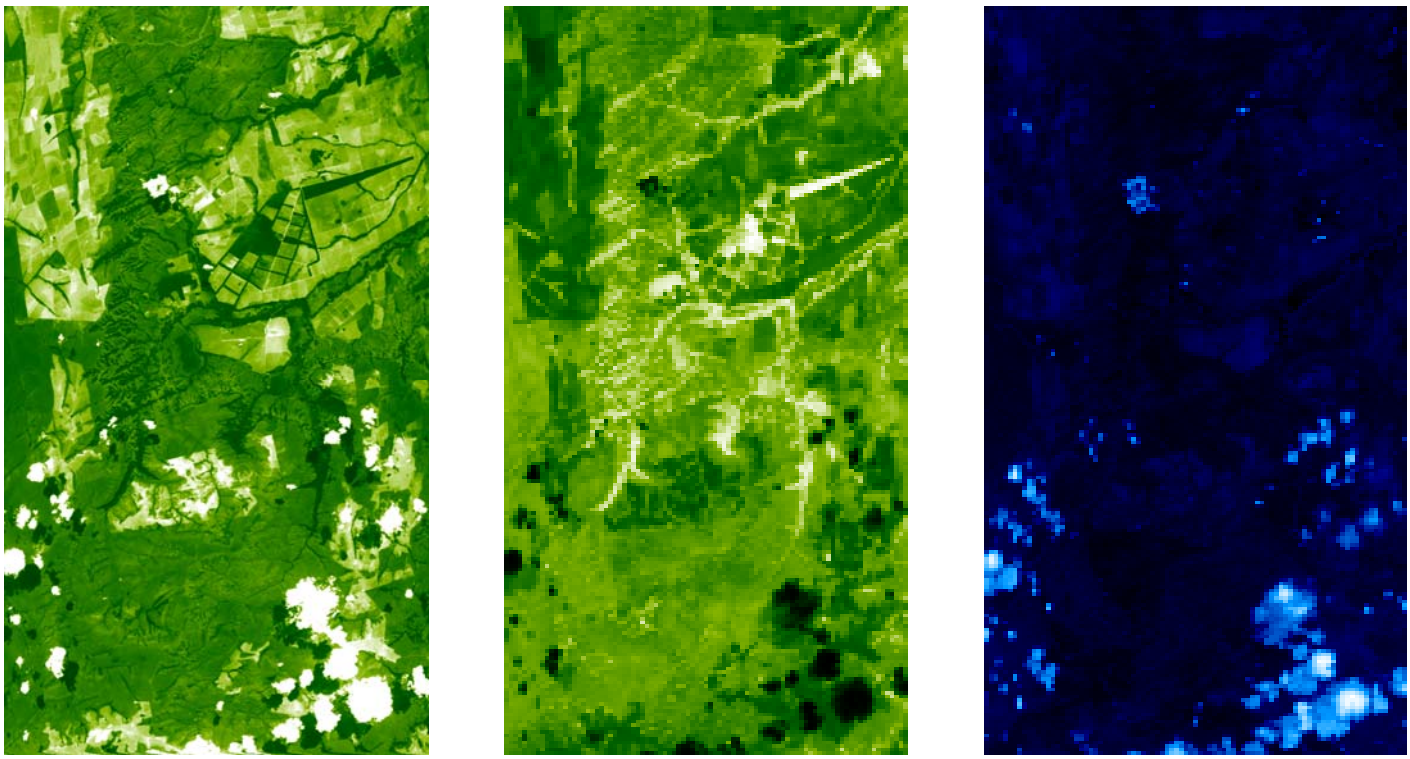

Figure 11: Reflectance images of Brazil scene from MAS/SCAR-B campaign ((a) Visible reflectance, (b) NDVI, (c) NDSI)

The range of the color scale for Figure 11a is from 0.0 to 0.2 in reflectance. The range for Figure 11b is from 0.05 to 0.7 in NDVI units. The range for Figure 11c is from -0.5 to 0.07 in NDSI units.

D43758, B. PDMO Released: 2010-06-22 (VERIFY REVISION STATUS)
PDMO

The NDSI/NDVI scatter plot for the Brazil scene is shown in Figure 12. Expected system performance errors were added to the scenes.

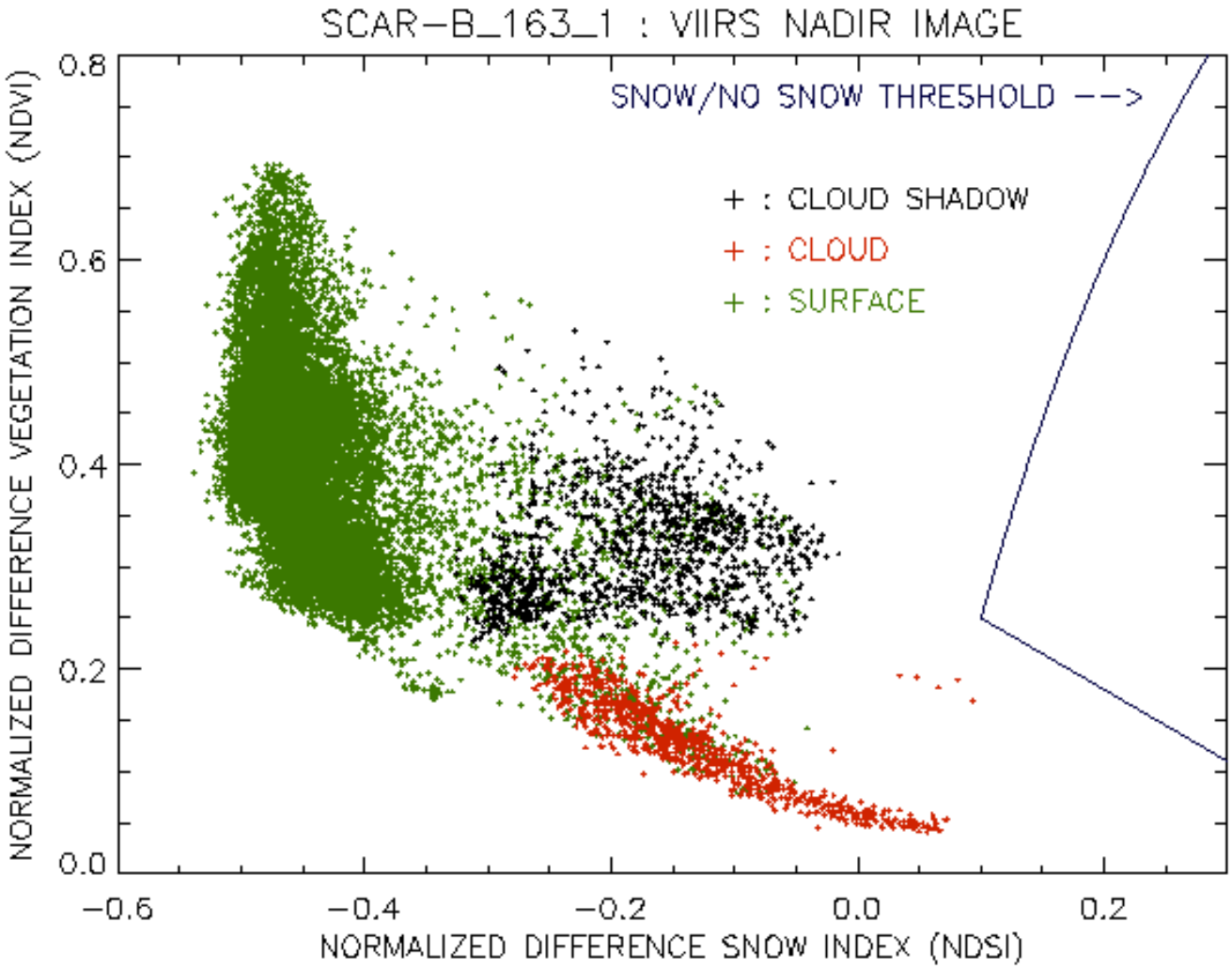

Figure 12: NDSI versus NDVI scatter plot of the MAS Brazil scene (SCAR-B_163_1).

Each data point in the Figure 12 scatter plot represents a VIIRS pixel at nadir, obtained by aggregating the MAS pixels to a VIIRS nadir pixel size. Correct classification occurs when pixels classified as snow fall to the right of the blue threshold boundary and when pixels classified as no snow fall to the left of the boundary. All pixels in this scene were correctly classified as no snow, including the cloud and cloud shadow pixels.

D43758, B. PDMO Released: 2010-06-22 (VERIFY REVISION STATUS)
PDMO

Minnesota Winter Scene: Visible (.645 μm) reflectance is shown in Figure 13a. Manual review of the ENVI-classified scene has established that the scene is 100% snow covered. The large variation in reflectance is caused by a variation in the forest canopy over the snow covered surface. The NDSI image is shown in Figure 13b. Brighter areas have larger NDSI. These areas have a lighter forest canopy. The NDVI image is shown in Figure 15c. Darker areas have larger NDVI. These areas have a denser forest canopy.

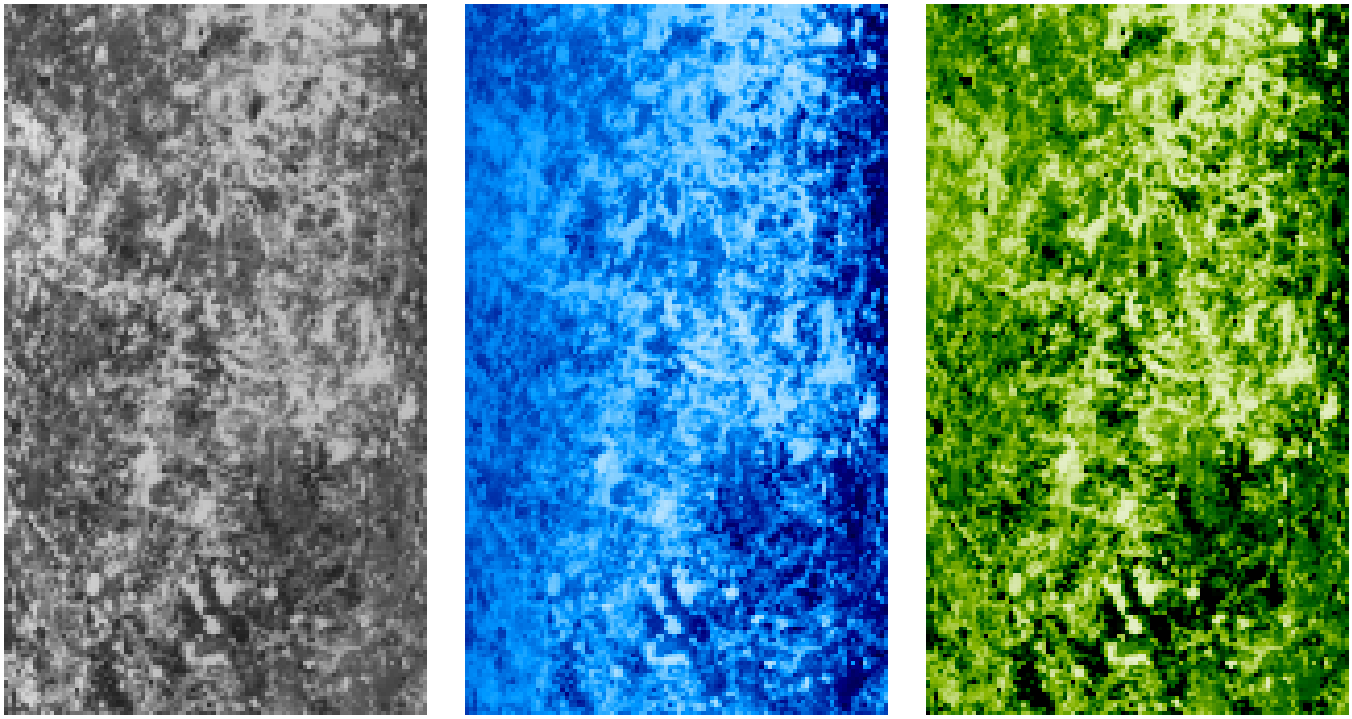

Figure 13. Reflectance images of Minnesota winter scene (MAS/WINCE campaign : (a) Visible reflectance, (b) NDSI, (c) NDVI)

The range of the gray scale for Figure 13a is from 0.0 to 1.0 in reflectance. The range of the color scale for Figure 13b is from NDSI = 0.0 (darkest) to NDSI = 0.8. The color scale for Figure 15c is reversed, from NDVI = 0.25 (darkest) to NDVI = 0.05.

D43758, B. PDMO Released: 2010-06-22 (VERIFY REVISION STATUS)
PDMO

The NDSI/NDVI scatter plot for the MAS Minnesota winter scene is shown in Figure 14. Expected system performance errors were added to the scene. All of the VIIRS pixels were correctly classified as snow.

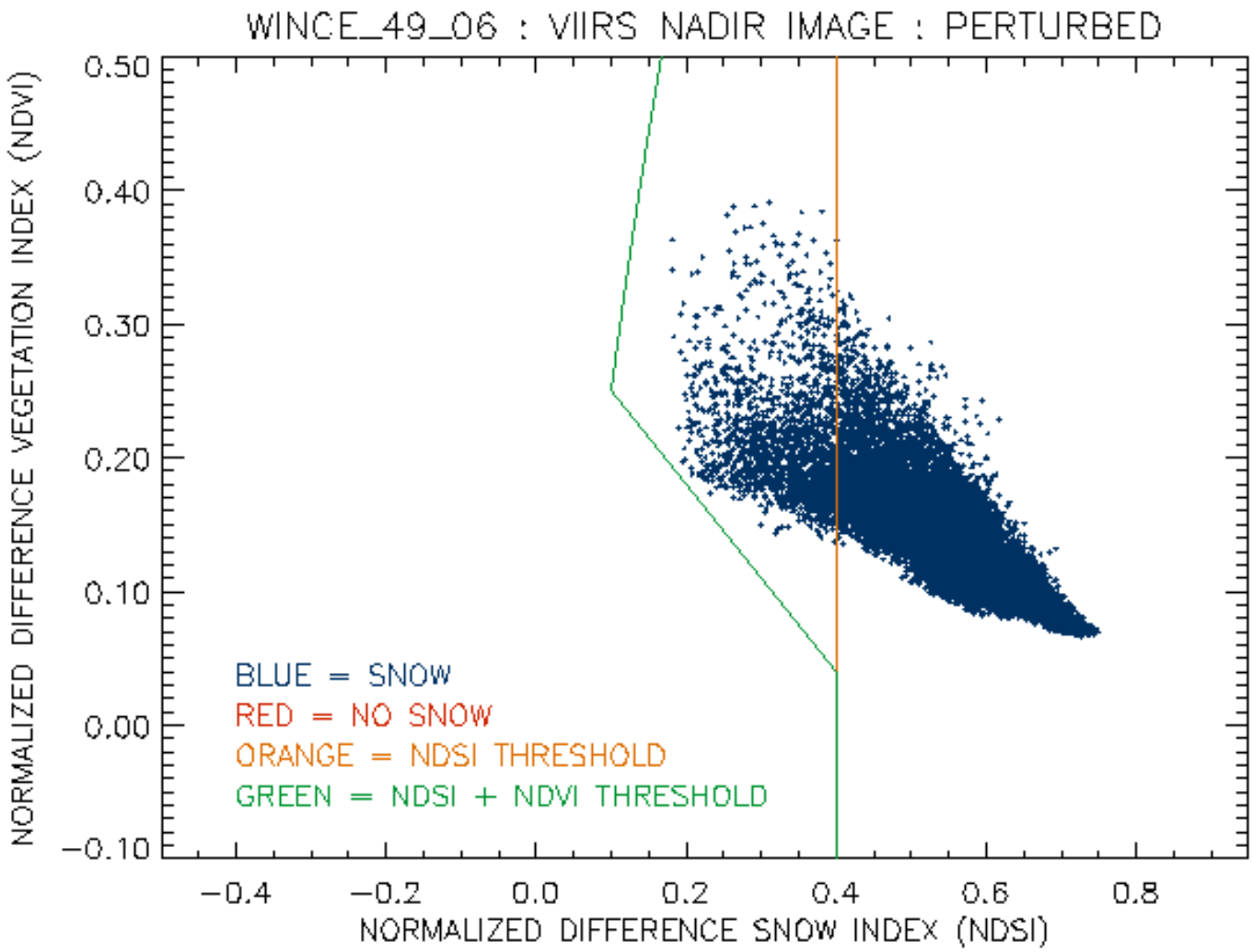

Figure 14: NDSI versus NDVI scatter plot of the MAS Minnesota winter scene (WINCE_49_06).

Each data point in the Figure 14 scatter plot represents a VIIRS pixel at nadir, obtained by aggregating the MAS pixels to a VIIRS nadir pixel size. Comparison of this figure to Figure 13 indicates that the scene can be characterized as a uniform snow-covered surface under a variable forest canopy. As the density of the canopy increases, the location in the scatter plot moves up and to the left, resulting in a canopy-density track. Correct classification occurs when pixels classified as snow (blue) fall to the right of the green threshold boundary and when pixels classified as no snow (red) fall to the left of the boundary. All pixels in this scene are correctly classified as snow. Without the NDVI correction, misclassification would occur where blue pixels fall to the left of the orange boundary, resulting in a correct classification of 91.6 %.

D43758, B. PDMO Released: 2010-06-22 (VERIFY REVISION STATUS)
PDMO

Colorado Winter Scene: Visible (.645 μm) reflectance is shown in Figure 15a. Manual review of the ENVI-classified scene has established that the scene has a mixture of snow cover. Aggregation of the classified pixels to a VIIRS nadir resolution produces a snow fraction "truth" image, shown in Figure 15b. The scene was perturbed by our model for system error, and our binary map algorithm applied to the perturbed data. The result is shown in Figure 17c.

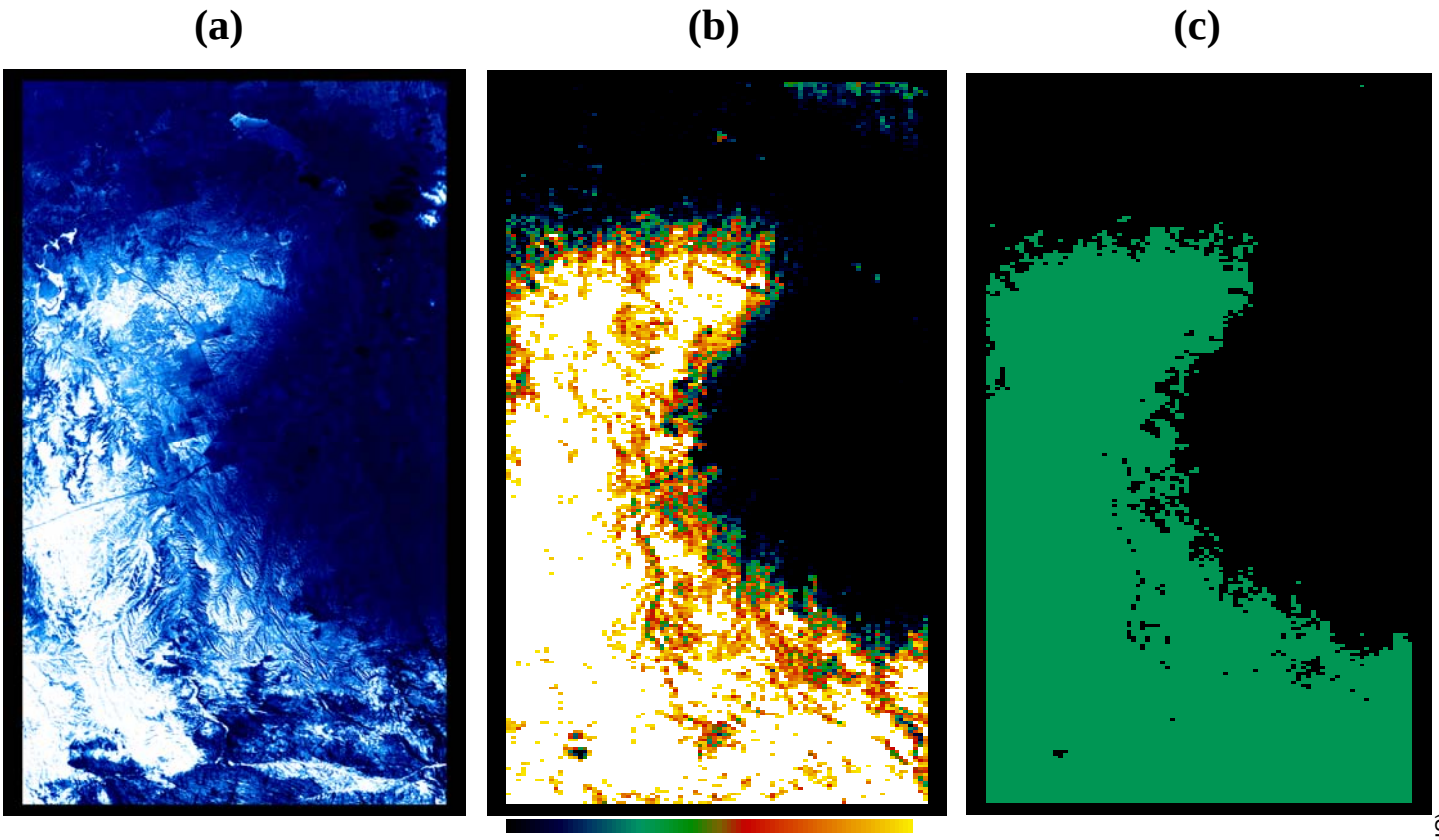

Figure 15. MAS Images of Eastern Colorado obtained on February 13, 1997.

Figure 15a shows the visible (0.648 micron) reflectance at 50 meter resolution. The extent of the scene is 35 km x 100 km. Figure 15b shows the snow fraction at 0.4 km resolution, obtained by classification and aggregation to a VIIRS pixel size at nadir. Figure 15c shows the output from the VIIRS snow binary map algorithm. System performance errors were used to simulate a VIIRS retrieval. Green cells are mapped as snow. 97.8 % of the pixels were correctly typed.

D43758, B. PDMO Released: 2010-06-22 (VERIFY REVISION STATUS)
PDMO

Figure 16 shows an NDSI versus NDVI scatter plot for the Colorado winter scene, aggregated to a VIIRS pixel size at nadir, with no error perturbations.

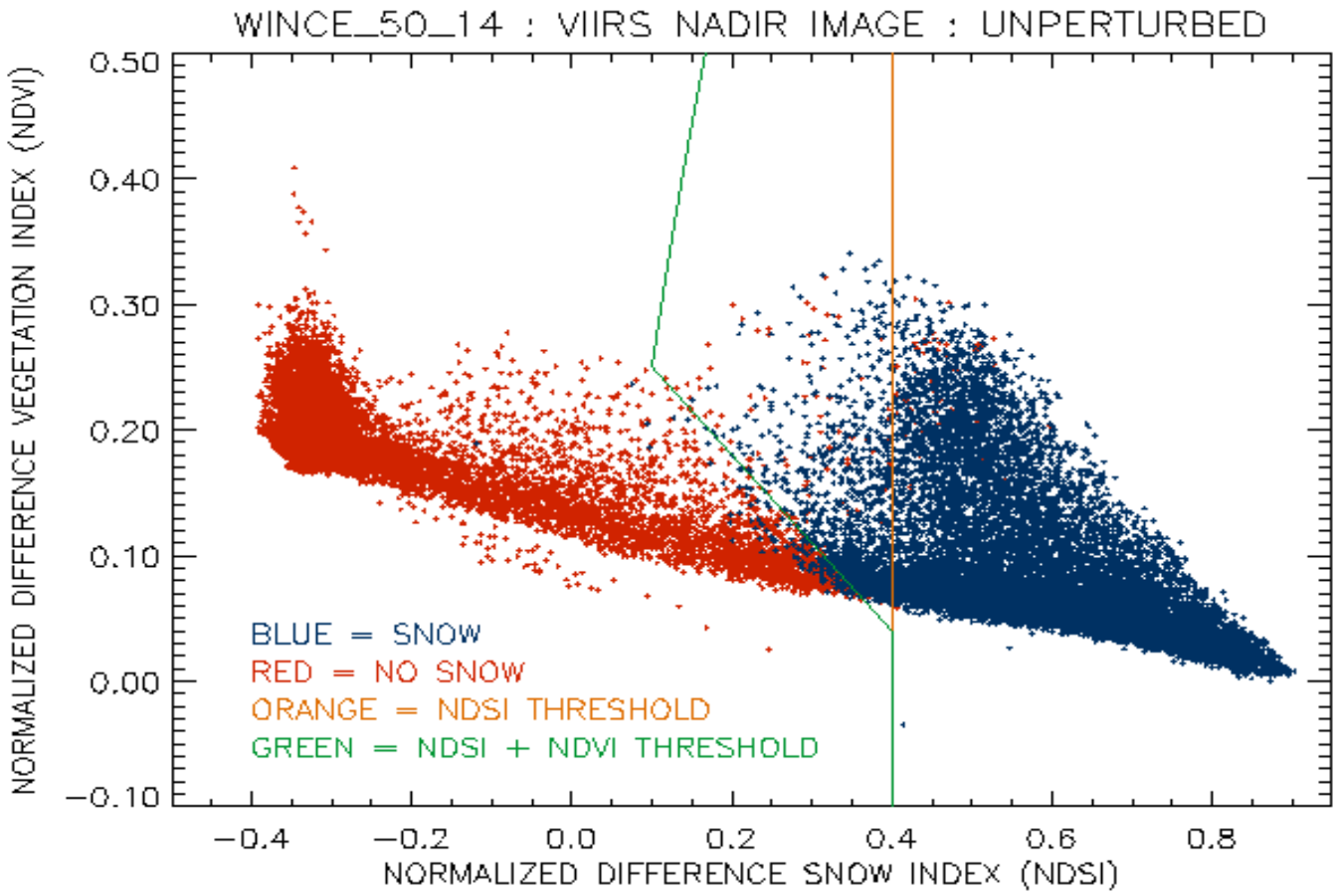

Figure 16: NDSI versus NDVI scatter plot of the MAS Colorado winter scene (WINCE_50_14).

Each data point in the Figure 16 scatter plot represents a VIIRS pixel at nadir, obtained by aggregating the MAS pixels to a VIIRS nadir pixel size. Correct classification occurs when pixels classified as snow (blue) fall to the right of the green threshold boundary and when pixels classified as no snow (red) fall to the left of the boundary. Correct classification occurs for 98.52 % of the pixels. Without the NDVI correction, additional misclassification would occur where blue pixels fall to the left of the orange boundary.

D43758, B. PDMO Released: 2010-06-22 (VERIFY REVISION STATUS)
PDMO

Figure 17 shows an NDSI versus NDVI scatter plot for the Colorado winter scene,, aggregated to a VIIRS pixel size at nadir, with error perturbations (atmospheric correction, sensor noise, sensor MTF, band misregistration) added.

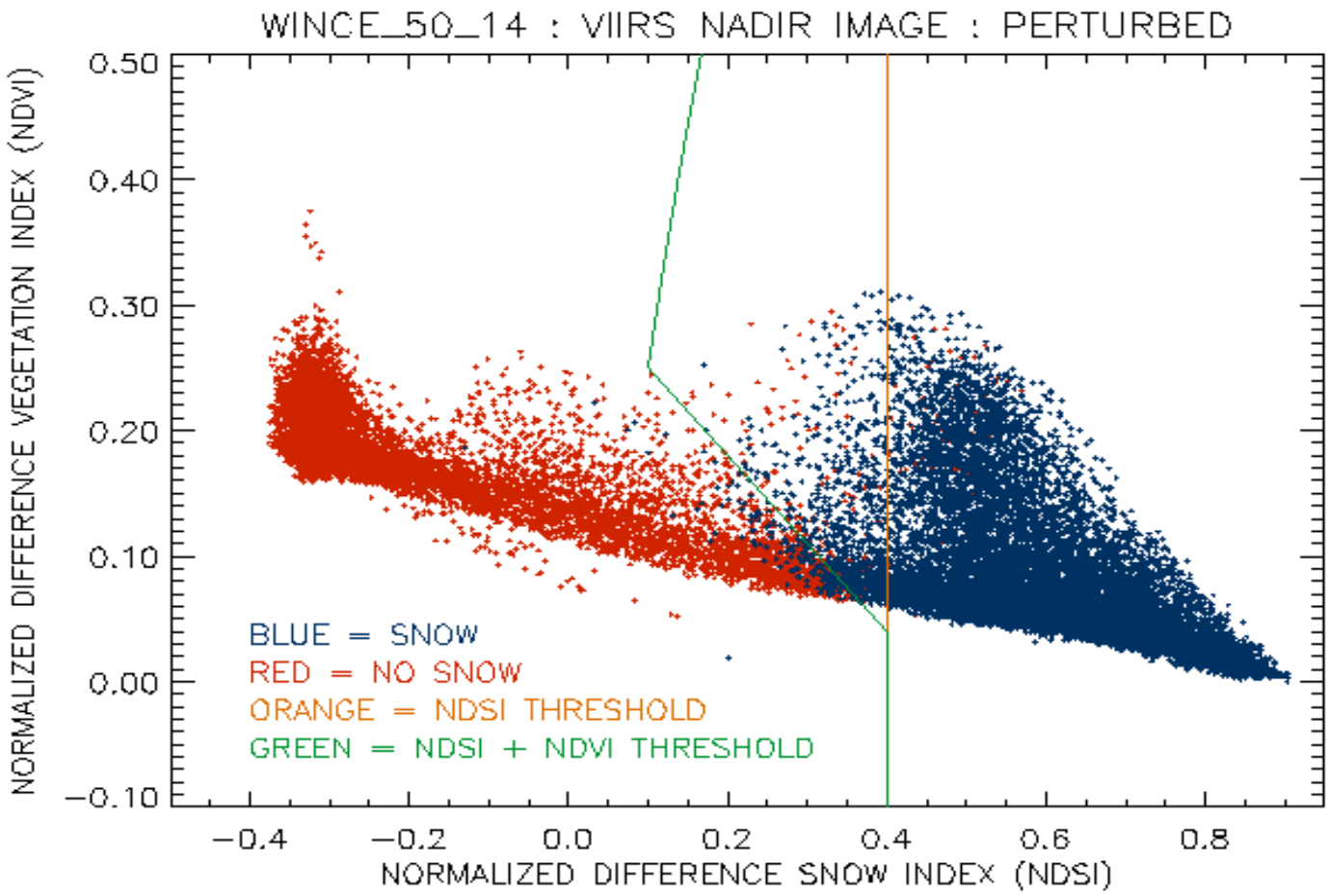

Figure 17: NDSI versus NDVI scatter plot the MAS Colorado winter scene (WINCE_50_14).

Each data point in the Figure 17 scatter plot represents a VIIRS pixel at nadir, obtained by aggregating the MAS pixels to a VIIRS nadir pixel size. Error perturbations have been added to the scene. Correct classification occurs when pixels classified as snow (blue) fall to the right of the green threshold boundary and when pixels classified as no snow (red) fall to the left of the boundary. Correct classification occurs for 97.79 % of the pixels. Without the NDVI correction, additional misclassification would occur where blue pixels fall to the left of the orange boundary.

D43758, B. PDMO Released: 2010-06-22 (VERIFY REVISION STATUS)
PDMO

The probability of correct typing for the Colorado winter scene is illustrated as a function of snow fraction truth in Figure 18.

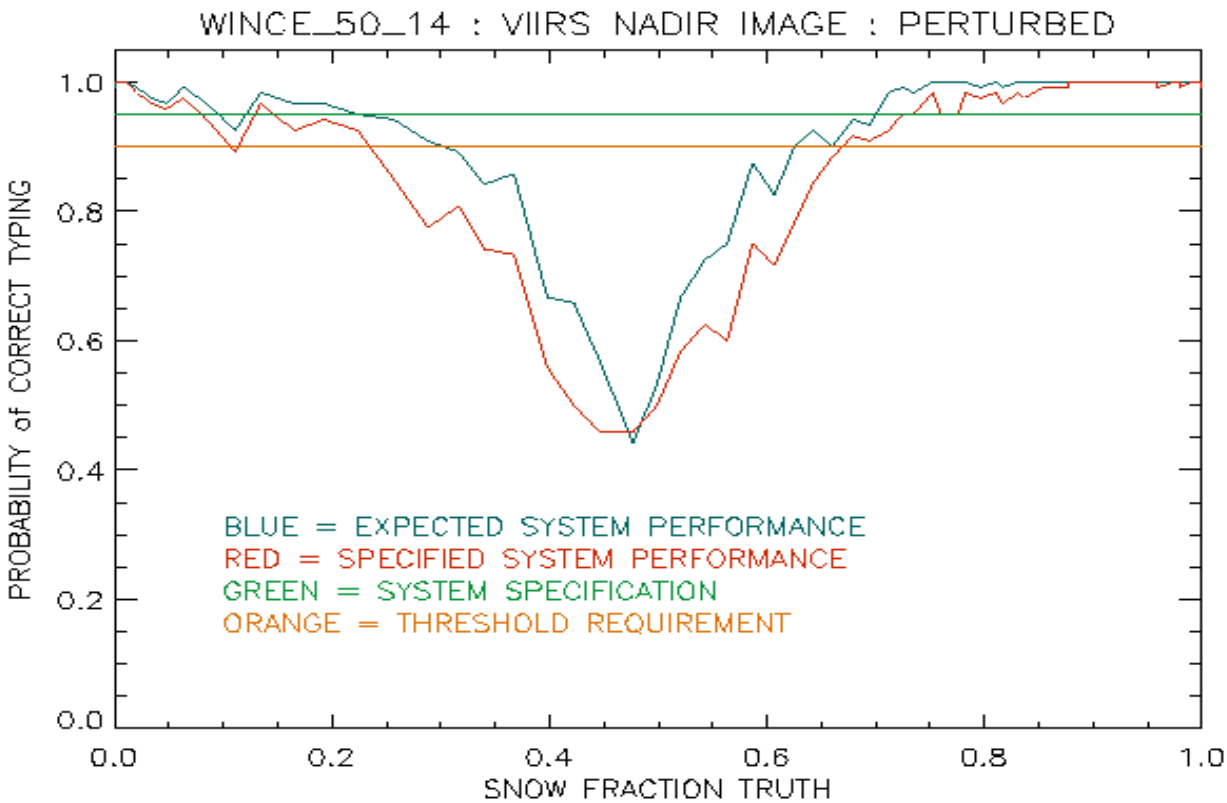

Figure 18: Probability of Correct Typing vs. Snow Fraction (MAS Colorado winter scene (WINCE_50_14))

Results from the analysis of the Colorado mixed snow cover scene have been incorporated into a stratified performance summary, shown in Table 4.

Table 4. Snow Binary Map Probability of Correct Typing (%)

	Snow Fraction (Truth)					Fraction of Mixed Pixels		
	0.0 – 0.2	0.2 – 0.4	0.4 – 0.6	0.6 – 0.8	0.8 – 1.0	10%	30%	50%
Specification	99.36	80.56	56.74	92.07	99.88	99.04	97.12	95.20
Performance	99.60	89.95	66.51	96.35	99.99	99.37	98.13	96.89

Table 4 applies for a nadir view, solar zenith angle = 60 degrees, some canopy, mixed snow/no snow.

An explanation of the stratification bins is in Section 4.1.1. Probability of correct typing for each of the "truth" bins was derived by examining the classification error for the subset of pixels falling into the

D43758, B. PDMO Released: 2010-06-22 (VERIFY REVISION STATUS)
PDMO

"truth" range of the given bin. Probability of correct typing for each of the "fraction of mixed pixels" bins was derived in the following manner. The probability of correct typing for pure pixels was calculated by examining the classification error for the subset of pure pixels. The probability of correct typing for mixed pixels was calculated by examining the classification error for the subset of mixed pixels. The probability of correct typing for a given fraction of mixed pixels is calculated as the weighted mean of the pure pixel and mixed pixel probabilities, with the mixed pixel weight equal to the fraction of mixed pixels.

It is important to note that the probability of correct typing for any binary classifier must approach 50% when the "truth" approaches 0.5. The performance results shown in Figure 18 and Table 4 reflect this characteristic. The practical measure of performance is for a realistic distribution of true fraction for various scenes, as is shown in the last three columns of Table 4.

4.2.1.2 Snow Binary Map Error Budgets

The various error sources have been incorporated into error budgets for easy, typical, and difficult cases. These are shown in Tables 5, 6, and 7.

Table 5. Error Budget for Retrieval of the Snow Binary Map EDR (Case 1)

SNOW COVER (Snow Binary Map) Case 1: Clear, Nadir, SZA = 60 degrees, 10% Mixed Pixels (Easy case)		
Specification v5 (CDR)	**Probability of Correct Typing (%)**	**Reference**
Threshold	90.00	VIIRS SRD
Objective	N/A	
System Specification	95.00	Raytheon VIIRS Specification v5
Predicted Performance	99.37	Raytheon VIIRS Specification v5
Margin	95.60	Raytheon VIIRS Specification v5
Algorithm Specification	99.55	Raytheon VIIRS Specification v5
Thresholds	99.58	Raytheon VIIRS Specification v5
Atmospheric Correction	99.98	Raytheon VIIRS Specification v5
Sensor Specification	99.81	Raytheon VIIRS Specification v5
Sensor Noise	99.96	Raytheon VIIRS Specification v5
MTF	99.84	Raytheon VIIRS Specification v5
Band Misregistration	99.85	Raytheon VIIRS Specification v5

D43758, B. PDMO Released: 2010-06-22 (VERIFY REVISION STATUS)
PDMO

Table 6. Error Budget for Retrieval of the Snow Binary Map EDR (Case 2)

SNOW COVER (Snow Binary Map) Case 2: Clear, Nadir, SZA = 60 degrees, 30% Mixed Pixels (Typical case)		
Specification v5 (CDR)	**Probability of Correct Typing (%)**	**Reference**
Threshold	90.00	VIIRS SRD
Objective	N/A	
System Specification	95.00	Raytheon VIIRS Specification v5
Predicted Performance	98.13	Raytheon VIIRS Specification v5
Margin	96.81	Raytheon VIIRS Specification v5
Algorithm Specification	98.67	Raytheon VIIRS Specification v5
Thresholds	98.74	Raytheon VIIRS Specification v5
Atmospheric Correction	99.93	Raytheon VIIRS Specification v5
Sensor Specification	99.43	Raytheon VIIRS Specification v5
Sensor Noise	99.89	Raytheon VIIRS Specification v5
MTF	99.52	Raytheon VIIRS Specification v5
Band Misregistration	99.55	Raytheon VIIRS Specification v5

Table 7. Error Budget for Retrieval of the Snow Binary Map EDR (Case 3)

SNOW COVER (Snow Binary Map) Case 3: Clear, Nadir, SZA = 60 degrees, 50% Mixed Pixels (Hard case)		
Specification v5 (CDR)	**Probability of Correct Typing (%)**	**Reference**
Threshold	90.00	VIIRS SRD
Objective	N/A	
System Specification	95.00	Raytheon VIIRS Specification v5
Predicted Performance	96.89	Raytheon VIIRS Specification v5
Margin	98.05	Raytheon VIIRS Specification v5
Algorithm Specification	97.80	Raytheon VIIRS Specification v5
Thresholds	97.91	Raytheon VIIRS Specification v5
Atmospheric Correction	99.89	Raytheon VIIRS Specification v5
Sensor Specification	99.04	Raytheon VIIRS Specification v5
Sensor Noise	99.82	Raytheon VIIRS Specification v5
MTF	99.20	Raytheon VIIRS Specification v5
Band Misregistration	99.25	Raytheon VIIRS Specification v5

D43758, B. PDMO Released: 2010-06-22 (VERIFY REVISION STATUS)
PDMO

If the various error sources listed in Tables 5, 6, and 7 were completely uncorrelated, the combination of probabilities would follow the formula:

$$P = P_1 \times P_2 \times \ldots \times P_N$$

Because the various error sources contain some correlation, the probabilities do not combine in this way. To derive the error budgets, we used multiple simulated images. Each simulated image contained one and only one of the perturbations. Comparison of retrieval with truth for each of the simulations gave us the error contribution of the associated perturbation. To simulate the easy, typical, and difficult cases, we computed separate errors for pure pixels and mixed pixels, and weighted accordingly.

The largest error is the “thresholds” error. This error is caused by the limitations of our limited threshold tests in accounting for the real variety of surface and canopy reflectance. In principle, the error could be reduced by improvements in canopy modeling and by the use of different thresholds for different surface types. Because our performance is significantly better than the requirement, we do not at present see the necessity to deviate from the MODIS approach.

Finally, we note that the sensor signal-to-noise performance is better than the specification. For the 1.6 micron band, the improvement is substantial. Because sensor noise is such a small component of the error budget, EDR performance would still meet specification if the sensor signal-to-noise were degraded to its specification values. For example, if we replace sensor noise performance with sensor noise specification, our probability of correct typing for our hard case degrades from to 96.88 % to 95.20 %, which meets our specification even for the hard case (c.f. Table 7).

4.2.1.3 Post-CDR

Following the Critical Design Review, there has been some minor development of the snow binary map algorithm, principally by the addition of the thermal mask. The MAS scenes used for pre-CDR verification did not show any false snow detection in the Brazil (SCAR-B) scene, so the addition of a thermal mask would have made no difference.

We have added an additional snow test scene from MODIS Terra. MODIS Aqua is not as useful for testing of our algorithm, because the 1.6 micron data is poor and the MODIS Aqua algorithm now uses the 2.1 micron band in its place.

The MODIS Terra scene is used for an additional performance test with a full swath product. This enables us to test performance off-nadir.

D43758, B. PDMO Released: 2010-06-22 (VERIFY REVISION STATUS)
PDMO

We compared our test results for this scene with the MODIS SNOWMAP swath product. We found a 99.3% agreement between the VIIRS algorithm output and the MODIS product. Figure 19 shows the MODIS and VIIRS results.

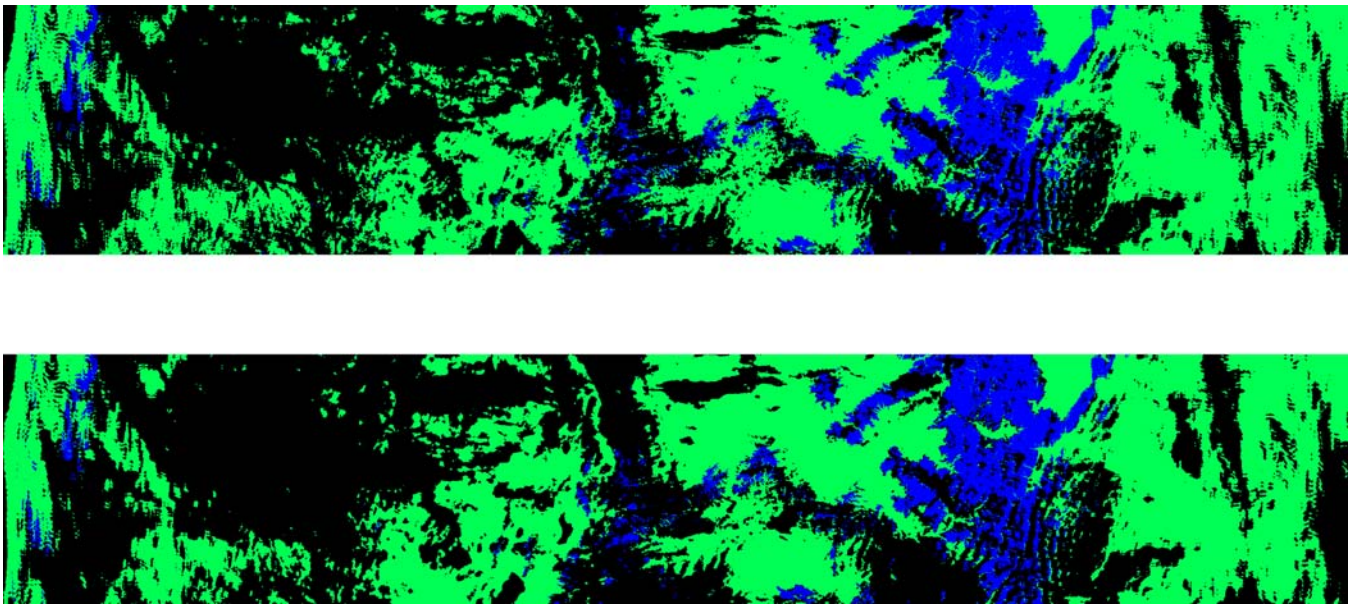

Figure 19: MODIS (top) and Unit Test (bottom) Snow Binary Map

In Figure 19, masked areas are black, NO SNOW is green, SNOW is blue. Note that these images are inverted, so that North is at the bottom and South is at the top.

4.2.2 Snow Fraction

4.2.2.1 Pre-CDR

Unlike the binary snow map algorithm, the snow fraction algorithm has undergone significant development since the Critical Design Review (CDR). Consequently, so of the pre-CDR performance analysis must be modified.

D43758, B. PDMO Released: 2010-06-22 (VERIFY REVISION STATUS)
PDMO

4.2.2.2 Snow Fraction Error Budget

The snow fraction error sources will correspond to those of the snow binary map since it is based on a 2x2 aggregation of the snow binary map.

4.3 LIMITS OF APPLICABILITY

In this section, we discuss the conditions under which our EDR specified performance cannot be attained.

4.3.1 Cloudy

The VIIRS Snow Cover EDR is required under clear conditions only, with clear defined as a cloud optical thickness less than 0.03. Our specification is for clear scenes only. Clouds are not amenable to spectral mixture analysis, because their reflectance properties are highly variable. The standard approach to minimize errors caused by clouds is to mask pixels where clouds are likely to be present in the radiance path. The VIIRS Cloud Mask *[Y2412]* will perform this function. Because no cloud mask is perfect, there will be some source of error caused by the effects of unmasked clouds. Thin clouds will perturb the upwelling surface reflected radiance by absorption and scattering, and will also be a source of reflected and emitted radiance unrelated to the surface. There will also be error due to incorrect classification of cloud-contaminated pixels as clear as well as due to cloud shadows.

It is desirable to perform tests to determine the expected size of the retrieval errors under various conditions of cloud optical thickness and phase. Thin cirrus clouds are a particularly important case of cloud error, because they are particularly difficult for the cloud mask to detect over snow. The conditions under which the specification cannot be attained may include a range of cloud optical thickness. The range will be determined by a balance between the increasing effect of clouds on the signal and the increasing probability of correct masking. The specification of this range has been deferred to future validation activity.

4.3.2 Low Light or Nighttime

The algorithm requires solar reflectance. Thermal contrast between snow and non-snow land surfaces is not a characteristic property. A solar zenith angle threshold of 70 degrees is adopted. For larger angles, surface reflectance errors become too large to guarantee the specification. Improved atmospheric correction would allow us to increase this threshold. The extension and refinement of the threshold is a goal of pre-launch initialization. MODIS experience will be of great value. Note that the EDR will be reported for solar zenith angles of 70-85 degrees, with a quality flag attached. AOT and thin clouds could affect where the solar zenith angle thresholds are set (c.f. Section 3.3.2).

D43758, B. PDMO Released: 2010-06-22 (VERIFY REVISION STATUS)
PDMO

4.3.3 Forest canopy (snow fraction)

A large part of snow cover occurs in the boreal forests. These forests obscure most of the underlying surface. Observations of forest canopy under conditions where 100 percent snow cover is expected to show albedo variations as large as 70%. Snow cover measurement uncertainties of 10% are not possible under these conditions. We have to be able to identify and flag pixels of forest canopy. The binary snow map algorithm will perform in boreal forests. We have verified its performance for the winter forest canopy of Northern Minnesota. Its performance in the deeper boreal forests is TBD. MODIS validation is expected to thoroughly characterize the performance in boreal forests.

4.4 PRACTICAL CONSIDERATIONS

4.4.1 Numerical Computation Considerations

The processing time for the VIIRS Snow Cover algorithm must be fast enough to meet the following NPOESS System Specification requirements:

> SYS002300 The System shall provide at least 95% (on a monthly average) of the (Snow Cover/Depth) EDR generated from the data collected by operational sensors on each NPOESS satellite to the Centrals in 28 minutes…per the EDR latency requirements specified in Appendix E of this specification. Class 1
>
> SYS002305 The latency of (the Snow Cover/Depth) EDR shall be less than 15 minutes at least 77% of the time on a monthly average. Class 1

This means that the VIIRS Snow Cover EDR must be completely processed from VIIRS raw data, including calibration and geolocation, within 28 minutes from the time the raw data are available. This requirement is a strong reminder that VIIRS is an operational instrument.

For the snow Cover EDR, the challenges posed by the latency requirement are minimal. The algorithm does not involve any kind of iteration or inversion of physically based models. The spectral unmixing method we use is not time intensive, as it reduces to a fixed number of tie point calculations with a single decision node.

4.4.2 Programming and Procedural Considerations

All procedures are automatic, to perform in the operational environment. The Snow Cover EDR will be produced in an integrated software system within the VIIRS Ground Segment of the IDPS. The algorithm is implemented by an independent testable software unit. The software design relevant to this unit is summarized in the VIIRS Context Level Software Architecture *[Y2469]*, Snow Ice Module Level Software Architecture *[Y2477]*, and Snow Cover Unit Level Detailed Design *[Y3234]*. The design will be tested at the system level as described in the most recent versions of the VIIRS Algorithm Design Verification Plan *[Y3236]*, Algorithm Software Integration and Test Plan *[Y3237]*, and System Verification and Validation Plan *[Y3270]*. A summary of the ultimate strategy for operational application of the system of VIIRS algorithms is provided in the VIIRS Operations

D43758, B. PDMO Released: 2010-06-22 (VERIFY REVISION STATUS)
PDMO

Concept document *[Y2468]*. The VIIRS Interface Control Document (ICD *[Y2470]*) provides more detail on the specifics of ancillary data requirements for VIIRS EDR products.

4.4.3 Configuration of Retrievals

The algorithm requires the availability of input data from a variety of sources, including VIIRS SDRs, VIIRS IPs, and a number of LUTs. A detailed list of these sources can be found in the Snow Ice Module Level Software Architecture *[Y2477]* and Snow Cover Unit Level Detailed Design *[Y3234]*. The EDR output is used as input to the Surface Reflectance and Surface Type algorithms in the VIIRS system. The NPOESS/VIIRS processing configuration is designed to satisfy these expectations *[Y2469].*

4.4.4 Quality Assessment and Diagnostics

Quality flags will be attached to each imagery resolution pixel and each moderate resolution pixel (c.f. Section 3.3.2). The snow fraction algorithm will produce an error estimate for each pixel. The algorithm should be expected to archive the final pixel errors for quality assessment. Ideally, a pixel error greater than an accepted threshold will be flagged. A detailed description of the quality flags can be found in the Snow Cover Unit Level Detailed Design *[Y3234],* the VIIRS Snow Cover Operational Algorithm Description Document *[D39593]* and the Common Data Format Control Book *[D34862-08]*.

4.4.5 Exception Handling

The software is designed to handle a wide variety of processing problems, including bad and missing data and fatal errors. In the event that processing problems prevent the production of useful EDR data, error flag information will be written to the output EDR file as metadata. A detailed description can be found in the Snow Cover Unit Level Detailed Design *[Y3234]*.

4.5 VALIDATION

Validation of the Snow Cover EDR will be conducted as part of the VIIRS System Verification and Validation Plan *[Y3270].* It will benefit greatly from MODIS data and MODIS validation experience.

The overall approach to validation will involve a multi-sensor, multi-temporal, regional approach comparing the VIIRS-derived snow cover with snow cover data from a variety of sources. One of the main goals of the validation is to quantify the errors associated with snow cover retrievals under a wide range of snow cover conditions. The variety of snow conditions in this validation scheme will cover all the snow classification categories described by Sturm et al. (1995) as shown in Table 8.

D43758, B. PDMO Released: 2010-06-22 (VERIFY REVISION STATUS)
PDMO

Table 8. Categories of snow cover and climate parameters

Snow Class	Windspeed	Temperature	Precipitation
Tundra	High	Low	Low
Taiga	Low	Low	Low
Prairie	High	High	Low
Maritime	Low-to-high	High	High
Alpine	Low	High	Low-to-high
Ephemeral	Low-to-high	Very high	Low

Figure 20 (from Sturm et al., 1995) shows the spatial distribution of snow cover classes in the northern hemisphere. Several regions representing each snow cover type will be selected and analyzed to quantify the mapping errors associated with each. Recognizing that these snow cover classes and solar illumination conditions vary over the course of the snow season it will be important to track the VIIRS snow cover EDR for each validation region over a full snow season from first accumulation to the date of snow disappearance.

Comparisons will be made between the VIIRS snow cover and other established snow cover products including the MODIS SNOMAP product, the NOAA IMS snow cover product, the SSM/I snow cover product, and the AMSR snow cover product. In addition, comparisons will be made between VIIRS snow cover and a new on-demand snow product that uses MODIS reflectances in a multiple snow end members in a linear spectral unmixing approach to compute sub pixel snow cover (e.g. Painter et al., 2003). This latter product is a NASA-funded effort produced by a multi-institution consortium headed by the UCSB snow hydrology group. The VIIRS snow cover validation effort will establish and maintain communication with the NASA, NOAA, and UCSB snow groups during the pre-launch phase and continue close collaboration and exchange of ideas and data during the post-launch phase.

D43758, B. PDMO Released: 2010-06-22 (VERIFY REVISION STATUS)
PDMO

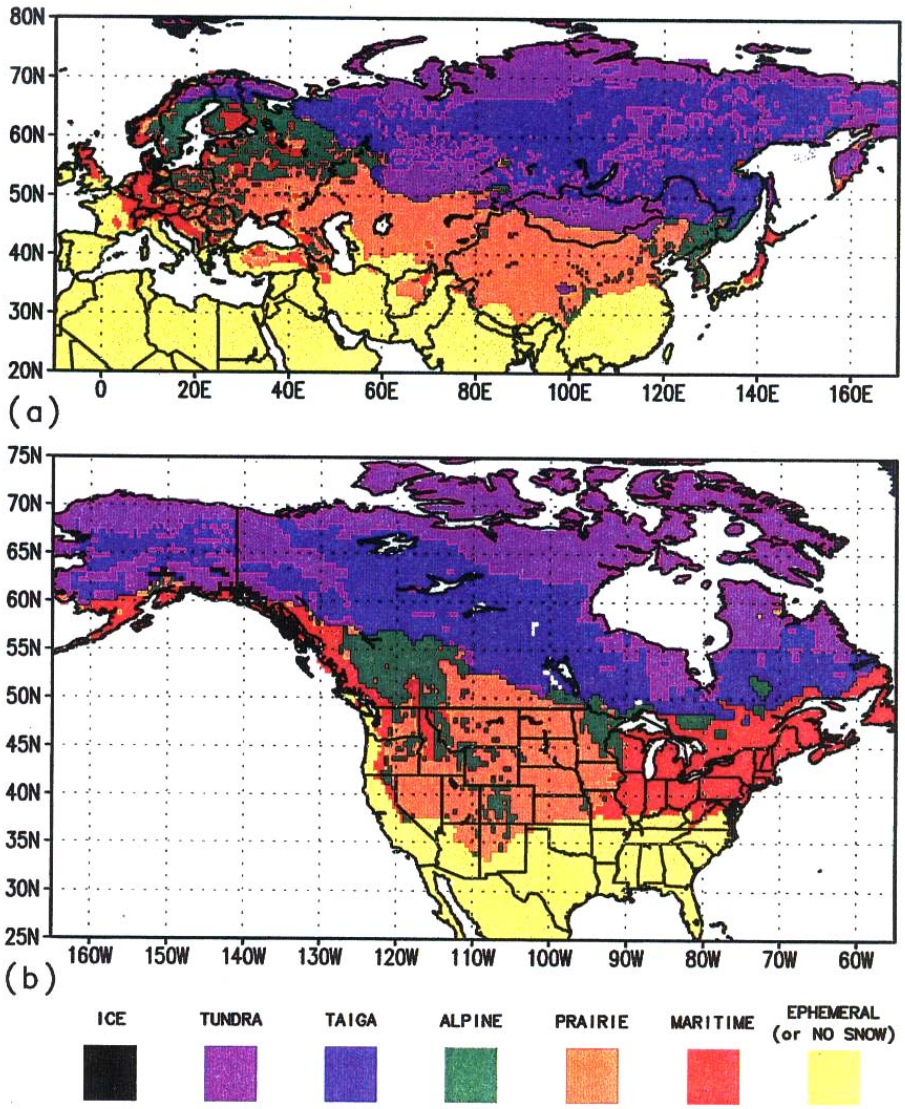

Figure 20. Northern hemisphere snow cover classification from Sturm et al. (1995)

D43758, B. PDMO Released: 2010-06-22 (VERIFY REVISION STATUS)
PDMO

The pre-launch plan includes sensitivity studies, analysis of simulated VIIRS data, and verification using MODIS data. Our plan is to maintain close contact with the MODIS science teams to coordinate our initialization activity with their post-launch validation. Observations from AVIRIS, MAS, LANDSAT ETM+, MODIS, GLI, and NPP/VIIRS will be used in the pre-launch phase to study the error characteristics and optimum techniques for the algorithm. It is expected that MODIS validation data will be of great value. MODIS/AMSR data can be used to investigate prospects for VIIRS/CMIS data fusion, and for cross-validation of the VIS/IR algorithm. The NPP/VIIRS will be critical in adjusting and verifying the values of the parameters in our LUTs. This process will be essential in making the algorithm operational prior to the NPOESS mission. We recommend an NPP/VIIRS validation campaign that includes *in situ* field measurements, ER-2 under flights (AVIRIS and MAS), and low level aircraft measurements at spatial resolutions as fine as 10 meters (e.g. RC-10 camera data). NPP/VIIRS data can be re-processed many times with various combinations of band weight functions and reflectance thresholds, and resulting snow retrievals can be compared to “truth” established from the auxiliary data. In this way, optimum band weight functions and reflectance thresholds can be selected.

Our plan is designed to interface smoothly with post-launch validation activity. The availability of NPP/VIIRS data prior to the NPOESS mission will be of enormous benefit. We would propose to conduct an NPP/VIIRS validation campaign similar to the MODIS validation activity, and use it as a model for the post-launch NPOESS/VIIRS validation campaign. In this sense, post-launch validation will already have been simulated by the pre-launch validation activity. Following launch, we would substitute real VIIRS data for the pre-launch simulated data. Cross-validation with NPOESS/CMIS provide a valuable extra capability.

D43758, B. PDMO Released: 2010-06-22 (VERIFY REVISION STATUS)
PDMO

5.0 ASSUMPTIONS

The statements and conclusions in this document are subject to the validity of the following assumptions:

1. An effective cloud mask over snow and ice surfaces will be available from the VIIRS Cloud Mask algorithm *[Y2412]*.

2. Pixels subject to large forest canopy errors can be identified and flagged.

6.0 REFERENCES

Ackerman, S. *et al.* (1997). Discriminating clear sky from cloud with MODIS. 1997.ATBD MOD-06. *http://eospso.gsfc.nasa.gov/atbd/modistables.html*

Barton, J.S., D.K. Hall, and G.A. Riggs, (2001). "Thermal and geometric thresholds in the mapping of snow with MODIS.", draft (http://modis-snow-ice.gsfc.nasa.gov/pap_therm.html)

Bohren, C.F., and B.R. Barkstrom (1974). Theory of the optical properties of snow. *J. Geophys. Res.*, 79, 4527-4535.

Bromwich, D.H. and R.-Y. Tzeng (1994). Simulation of the modern arctic climate by the NCAR CCM1. *J. Climate***,** 7, 1050-1069.

Carroll, T.R., J.V. Baglio, Jr., J.P. Verdin, and E.W. Holroyd, III (1989). Operational mapping of snow cover in the United States and Canada, using airborne and satellite data. *Proceedings of the 12th Canadian Symposium on Remote Sensing,* V. 3, IGARSS '89, 10-14 July 1989, Vancouver, Canada.

Carroll, T.R., (1990). Operational airborne and satellite snow cover products of the National Operational Hydrologic Remote Sensing Center. *Proceedings of the 47th annual Eastern Snow Conference,* June 7-8, 1990, Bangor, Maine, CRREL Special Report 90-44.

Chang, A.T.C. (1998). AMSR-based SWE retrieval algorithm ATBD. *http://wwwghcc.msfc.nasa.gov/AMSR/snow_ATBD*

Chang, A.T.C., J.L. Foster and D.K. Hall, (1987). Microwave snow signatures (1.5 mm to 3 cm) over Alaska, *Cold Regions Science and Technology*, 13, pp 153-160.

Chang, A.T.C. *et al.* (1987). Estimating snowpack parameters in the Colorado River basin. International Association of Hydrological Sciences Publication 166 (Symposium at Vancouver 1987 – *Large Scale Effects of Seasonal Snow Cover*), 343-352.

D43758, B. PDMO Released: 2010-06-22 (VERIFY REVISION STATUS)
PDMO

Crane, R.G. and M.R. Anderson (1984). Satellite discrimination of snow/cloud surfaces. *Intl. J. Remote Sens*., 5(1), 213-223.

Dozier, J., S.R. Schneider and D.F. McGinnis Jr., 1981: Effect of grain size and snowpack water equivalence on visible and near-infrared satellite observations of snow. *Water Resources Research*, 17, pp 1213-1221.

Dozier, J. (1984). Snow reflectance from Landsat-4 Thematic Mapper. *IEEE Trans. Geosci. Remote Sens.*, 22(3), 323-328.

Dozier, J. (1989). Spectral signature of alpine snow cover from the Landsat Thematic Mapper. *Remote Sens. Environ*., 28, 9-22.

Foster, J.L., D.K. Hall, A.T.C. Chang and A. Rango, 1984: An overview of passive microwave snow research and results, *Reviews of Geophysics*, 22, pp 195-208.

Foster, J.L., and A.T.C. Chang (1993). Snow cover. In *Atlas of Satellite Observations Related to Global Change* R.J. Gurney, C.L. Parkinson, and J.L. Foster (eds.), Cambridge University Press, Cambridge, pp. 361-370.

Foster, J.L., A.T.C. Chang, and D.K. Hall (1997). Comparison of snow mass estimates from a prototype passive microwave snow algorithm, a revised algorithm, and a snow depth climatology. *Remote Sens. Environ.,* 62, 132-142.

Grenfell, T.C., D.K. Perovich, and J.A. Ogren (1981). Spectral albedos of an alpine snowpack. *Cold Regions Sci. Technol*., 4, 121-127.

Grody, N.C., and A.N. Basist (1996). Global identification of snow cover using SSM/I instruments. *IEEE Trans. Geosci. Remote Sens.*, 34(1), 237-249.

Hall, D.K., A.Tait, G. Riggs, and V. Salomonson (1998). MODIS: Snow mapping Algorithm and the Sea Ice Mapping Algorithm (Version 4.0). ATBD-MOD-10. *http://eospso.gsfc.nasa.gov/atbd/modistables.html*

Hall, D.K., et al. (2001). Algorithm Theoretical Basis Document (ATBD) for the MODIS Snow and Sea Ice-Mapping Algorithms. http://snowmelt.gsfc.nasa.gov/MODIS_Snow/atbd01.html

Hoffer, R.M. (1978). Biological and physical considerations in applying computer-aided analysis techniques to remote sensor data. In *Remote Sensing: The Quantitative Approach* (P.H. Swain and S.M. Davis, eds.). New York: McGraw-Hill.

Klein,A.G., D.K. Hall, and G.A. Riggs (1998). Improving snow-cover mapping in forests through the use of a canopy reflectance model. *Hydrological Processes*, 12(10-11): 1723-1744.

Klein, A.G., D.K. Hall and A. Nolin, 2001: Development of a prototype snow albedo algorithm for the NASA MODIS instrument, Proceedings of the 57th Eastern Snow Conference, 17-19 May 2000, Syracuse, NY.

D43758, B. PDMO Released: 2010-06-22 (VERIFY REVISION STATUS)
PDMO

Klein, A.G. (2001). "Development of a Prototype Snow Albedo Algorithm for the NASA MODIS Instrument," *Hydrological Processes,* submitted.

Kou, L, D. Labrie, and P. Chylek, Refractive index of ice in the 1.4 – 7.8 mm spectral range, Appl. Opt., 32, 3531-3540, 1993.

Matson, M., (1991). NOAA satellite snow cover data. *Palaeogeography, Palaeoclimatology, Palaeoecology*, 90: 213-218.

Matson, M., C.F. Roeplewski, and M.S. Varnadore (1986*). An Atlas of Satellite Derived Northern Hemisphere Snow Cover Frequency.* National Weather Service, Washington, D.C. 75pp.

Nolin, A.W., J. Dozier, and L.A.K. Mertes (1993). Mapping alpine snow using a spectral mixture modeling technique. *Annals of Glaciology,* 17, 121-124.

Nolin, A. W., and J. C. Stroeve (2000). Validation studies and sensitivity analyses for retrieval of snow albedo from EOS AM-1 instruments: Progress report for 1999-2000 work. May 20,2000, http://www-nsidc.colorado.edu/PROJECTS/ALBEDO

Painter, T.H., D.A. Roberts, R.O. Green, and J. Dozier (1998). The effect of grain size on spectral mixture analysis of snow covered area from AVIRIS data. *Remote Sens. of Environ.,* 65(3): 320-332.

Planet, W.G. (ed.), (1988). Data extraction and calibration of TIROS-N/NOAA radiometers. NOAA Technical Memorandum NESS 107 – Rev. 1, Oct. 1988. 130 pp.

Ramsay, B., 1998: The interactive multisensor snow and ice mapping system, *Hydrological Processes*, 12:1537-1546.

Rango, A., 1993: Snow hydrology processes and remote sensing, Hydrological Processes, 7:121-138.

Rango, A. and J. Martinec, 1982: Snow accumulation derived from modified depletion curves of snow coverage, Symposium on Hydrological Aspects of Alpine and High Mountain Areas, IAHS Publication No. 138:83-90.

Roberts, D.A., M. Gardner, R. Church, S. Ustin, G. Scheer, and R.O. Green (1998). Mapping Chaparral in the Santa Monica Mountains Using Multiple Endmember Spectral Mixture Models. *Remote Sens. of Environ.,* 65(3): 267-279.

Rosenthal, W.C. (1993). Mapping mountain snow cover at sub pixel resolution from the Landsat Thematic Mapper. Master's thesis, Univ. Calif. at Santa Barbara.

Rosenthal, W.C., and J. Dozier (1996). Automated mapping of mountain snow cover at sub pixel resolution from the Landsat TM. *Water Resources Res.,* 31(1), 115-130.

Stamnes, K., S-C. Tsay, W. Warren, and K. Jayaweera, Numerically stable algorithm for discrete-ordinate-method radiative transfer in multiple scattering and emitting layered media, Appl. Opt., 27, 2502-2509, 1988.

D43758, B. PDMO Released: 2010-06-22 (VERIFY REVISION STATUS)
PDMO

Vermote, E. (1999). MODIS: Atmospheric Correction Algorithm Spectral Reflectances, ATBD-MOD-08. *http://eospso.gsfc.nasa.gov/atbd/modistables.html*

Vermote E., D. Tanre, J. L. Deuze, M. Herman, and J. J. Morcrette, Second Simulation of the Satellite Signal in the Solar Spectrum, 6S User Guide, Version 2, 218pp. 1997.

Warren, S.G. (1982). Optical properties of snow. *Rev. Geophys. Space Phys*., 20(1), 67-89.

Warren, S. G., Optical constants of ice from the ultraviolet to the microwave, Appl. Opt., 23, 1206-1225, 1984.

Warren, S.G., and W.J. Wiscombe (1980). A model for the spectral albedo of snow. II. Snow containing atmospheric aerosols, *J. Atmos. Sci.,* 37(12), 2734-2745.

Winther, J.G., 1992: Landsat thematic mapper (TM) derived reflectance from a mountainous watershed during the snow melt season, *Nordic Hydrology*, 23, pp 273-290.

Wiscombe, W.J., and S.G. Warren (1980). A model for the spectral albedo of snow,1,pure snow*. J. Atmos. Sci.,* 37(12), 2712-2733.

D43758, B. PDMO Released: 2010-06-22 (VERIFY REVISION STATUS)
PDMO